

Bounds on the bubble wall velocity

Wen-Yuan Ai,^{*1} Benoit Laurent^{†2} and Jorinde van de Vis^{‡3}

¹*Theoretical Particle Physics and Cosmology, King's College London,
Strand, London WC2R 2LS, United Kingdom*

²*McGill University, Department of Physics, 3600 University St.,
Montréal, QC H3A2T8 Canada*

³*Theoretical Physics Department, CERN,
1 Esplanade des Particules, CH-1211 Geneva 23, Switzerland*

Abstract

Determining the bubble wall velocity in first-order phase transitions is a challenging task, requiring the solution of (coupled) equations of motion for the scalar field and Boltzmann equations for the particles in the plasma. The collision terms appearing in the Boltzmann equation present a prominent source of uncertainty as they are often known only at leading log accuracy. In this paper, we derive upper and lower bounds on the wall velocity, corresponding to the local thermal equilibrium and ballistic limits. These bounds are completely independent of the collision terms.

For the ballistic approximation, we argue that the inhomogeneous plasma temperature and velocity distributions across the bubble wall should be taken into account. This way, the hydrodynamic obstruction previously observed in local thermal equilibrium is also present for the ballistic approximation. This is essential for the ballistic approximation to provide a lower bound on the wall velocity. We use a model-independent approach to study the behaviour of the limiting wall velocities as a function of a few generic parameters, and we test our developments in the singlet extended Standard Model.

*wenyuan.ai@kcl.ac.uk

†benoit.laurent@mail.mcgill.ca

‡jorinde.van.de.vis@cern.ch

Contents

1	Introduction	2
2	A brief review of bubble wall dynamics and hydrodynamics	5
2.1	Coupled scalar and plasma equations of motion	6
2.2	The standard matching conditions and fluid equations	8
3	Bubble wall velocity in the LTE and ballistic approximations	10
3.1	The LTE approximation	10
3.2	The ballistic approximation	10
4	Demonstration that LTE and ballistic provide bounds on the wall velocity	14
4.1	LTE as upper bound on the wall velocity in the template model	14
4.2	Demonstration that LTE and ballistic approximations bound v_w in the linearized Boltzmann equation	16
5	Comparison between LTE and ballistic results	19
5.1	Model-independent analysis	20
5.1.1	Results	21
5.1.2	Large mass limit	27
5.2	Example model: the Standard Model coupled to a gauge singlet	30
6	Conclusions	32
A	Model-independent hydrodynamics with the template EoS	35
B	Ballistic pressures for Bose-Einstein and Fermi-Dirac distributions	37
C	Particles that lose mass when entering the bubble	37

1 Introduction

First-order phase transitions (FOPTs) are common phenomena in daily life but are also naturally predicted to have occurred in the early Universe by many models beyond the Standard Model (SM). See, e.g., Refs. [1–40] for a far from complete list of examples. FOPTs are interesting not only because they can generate a stochastic background of gravitational waves (GWs) [41–45], but also because they have far-reaching phenomenological applications. Among other possibilities, they may be relevant for explaining the cosmic matter-antimatter asymmetry [46–54] or the generation of dark matter [55–64].

Almost all the FOPT-related phenomena, as well as the generated GW signals, depend crucially on the bubble wall velocity v_w . For this reason, there have been a lot of works on bubble wall dynamics in recent years [65–91]. To determine v_w , one in principle needs to solve the coupled equation of motion (EoM) of the order-parameter scalar field and the Boltzmann equations for the particles that couple with the scalar field [92, 93]. See Refs. [75, 91, 94–98] for some studies following this approach. In [99–104] the backreaction of the fluid onto the expanding bubbles is incorporated by adding an effective friction term to the scalar field EoM.

Solving the Boltzmann equations and the scalar EoM is however challenging not only because they are coupled integrodifferential equations, but also because the computation of the collision terms suffers from large uncertainties. It is therefore highly desirable to derive the upper and lower bounds of the wall velocity with simpler approaches, which is the goal of the present work. Such upper and lower bounds can be very useful in the initial exploration of a BSM model. For example, certain dark matter generation mechanisms require bubbles with very slow walls [56, 57]. To find out whether a specific BSM realization can give successful dark matter generation, one might first determine the upper and lower bound for the wall velocity. These results can then motivate a more detailed computation of v_w , including a solution of the Boltzmann equations (or save one from wasting time and numerical resources).

Our estimates for the upper and lower bound of the wall velocity correspond to the two limiting cases for the deviation from equilibrium of the particles in the plasma. Intuitively, the larger the deviation from thermal equilibrium of the plasma, the greater the friction the bubble wall experiences. One can imagine (and we will demonstrate in this work) that the deviation from equilibrium is a monotonically decreasing function of the collision rate Γ for the particles in the plasma. Let us assume that the interaction strength is infinitely strong, i.e., $\Gamma \rightarrow \infty$, particles can instantaneously relax to their equilibrium state after being perturbed, and therefore, the plasma would remain in local thermal equilibrium as the wall passes through. This is the local thermal equilibrium (LTE) approximation [67, 71, 80], which can provide the lower bound of the friction experienced by the wall and the upper bound of the velocity. Although in LTE there is no *dissipative* friction, there is still a backreaction force due to hydrodynamic effects [99, 105], which could lead to a stationary motion of the wall. Such hydrodynamic effects are caused by the inhomogeneous temperature and velocity distributions near the wall. It was noted in Ref. [71] that in LTE, the wall velocity can be determined very simply and efficiently with a new matching condition in the hydrodynamic quantities across the bubble wall due to the conservation of entropy. This method has been more thoroughly studied in Ref. [80].

In the opposite limit, $\Gamma \rightarrow 0$, particles do not collide with each other, and the friction can be studied by analyzing particle transmission across the wall. This is the *ballistic* approximation that is usually used for ultra-relativistic bubble walls [106–112], but has also been applied for slow walls in Refs. [65, 88, 94]. In contrast to the LTE case, the inhomogeneity in the plasma temperature and velocity distributions is usually not considered in the ballistic approximation.¹ Without considering it, the crucial hydrodynamic effects are ignored and the estimate of the velocity could be misleading. In particular, it has been observed when solving the scalar EoM and

¹An exception is the recent work [88] which considers the inhomogeneous distribution in the temperature but not in the fluid velocity.

Boltzmann equations [68, 75] (see also Refs. [74, 113]), but also in a pure LTE analysis [80, 114] that the frictional pressure has a peak at the Jouguet velocity. Such a peak is important as it tells us that the friction is not a monotonous function of the wall velocity and thus one cannot simply use the asymptotic value of the friction in the ultrarelativistic limit [106] to determine whether a bubble wall runs away or not [114]. In this work, we carefully account for the mentioned inhomogeneity in the plasma temperature and velocity across the wall. As a result, we observe a similar pressure curve peaked at the Jouguet velocity for the ballistic approximation, and we can extract a lower bound on the wall velocity.

The goal of this work is three-fold:

- We update the ballistic approximation to account for the inhomogeneous temperature and velocity profile, promoting it such that it gives us a lower bound on v_w .
- We demonstrate that the ballistic approximation gives the upper bound of the friction (equivalently lower bound of the wall velocity), and the LTE approximation the lower bound.
- We demonstrate in practice how the bounds on the velocity can be applied to simple and realistic models.

In this paper, we will see a few different length scales for the phase transition (PT) dynamics. Here we summarise them in Table 1. The reader may refer to it when these length scales are introduced.

Length scale	Description	Typical value
Wall thickness L_w (wall frame)	Scalar fields' variation length scale	$1/m_\phi$
Mean free path L_{MFP} (plasma frame)	Plasma's thermalisation length scale	$1/\Gamma \sim 1/(g^n T)$
Bubble radius R_{bubble} (plasma frame)	Length scale of the macroscopic structures (e.g. shock and rarefaction waves, bubble)	$\mathcal{O}(1 - 10^{-5}) \times 1/H$
δ (wall frame)	Distance from the wall at which the scalar fields are constant	$\delta \gg L_w$ and $\delta \ll \gamma_w R_{\text{bubble}}$
δ' (wall frame)	Distance at which the plasma has reached its asymptotic equilibrium state	$\delta' \gg \max(\gamma_w L_{\text{MFP}}, L_w)$ and $\delta' \ll \gamma_w R_{\text{bubble}}$

Table 1: Summary of the different length scales relevant for the phase transition dynamics. m_ϕ is the scalar field's mass and g^n is some power of the coupling constant. We have also indicated in which frame these quantities are defined.

The remainder of this article is as follows. In the next section, we give a brief review of the general aspects of bubble wall dynamics and hydrodynamics. In Sec. 3 we discuss the two approximations used in this paper. We derive the ballistic distribution functions with hydrodynamics

correctly integrated and derive a new effective matching condition for the ballistic approximation. In Sec. 4, we argue that the LTE and ballistic limits establish bounds on the wall friction and velocity. In Sec. 5, we present our numerical results both for a model-independent analysis and for an example model. We conclude in Sec. 6. For completeness, some technical details are left in appendices. Throughout we use the metric signature $(+, -, -, -)$.

2 A brief review of bubble wall dynamics and hydrodynamics

We illustrate the bubble wall dynamics in Fig. 1, taking a deflagration as an example. The relevant quantities for a hydrodynamic description are the fluid temperature and velocity distributions, $T(\xi)$ and $v(\xi)$, where $\xi = r/t$ with r the radial coordinate and t the time since nucleation. Since there is no other scale in the problem, the solutions for v and T are self-similar, i.e., they only depend on ξ . The bubble wall and the shock front can be viewed as having zero size at the hydrodynamics scale. $T(\xi)$ and $v(\xi)$ are continuous, except at the bubble wall and the shock front. The quantities on both sides of these fronts (either the phase front, i.e. bubble wall, or shock front) are therefore related by matching conditions. To study the matching conditions at the wall and to determine the wall velocity, one needs to zoom in on the fronts to a scale where the wall has a finite width. One uses the coupled EoM between the scalar field and the plasma to find the matching conditions. There are two standard (hydrodynamic) matching conditions given by the conservation of the total energy-momentum tensor. For both of the two approximations adopted in this work, there is another matching condition with which one can fully determine the system for a given nucleation temperature T_n .

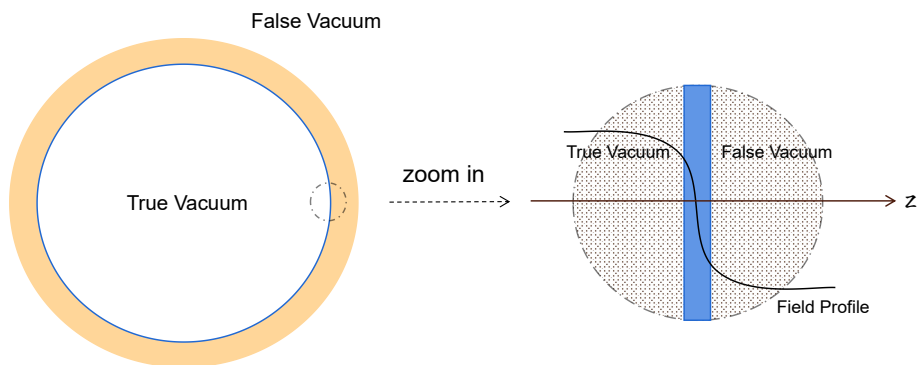


Figure 1: Sketch of bubble wall dynamics using the deflagration mode as an example. The bubble wall and shock front are viewed as having zero size at the hydrodynamic scale. The hydrodynamic quantities T and v are discontinuous at these fronts. To study the matching conditions, one then needs to zoom in on these fronts.

2.1 Coupled scalar and plasma equations of motion

The analysis of the friction on bubble walls is usually based on the following coupled EoMs for the background field and plasma [92–94],

$$\square\phi + \frac{dV(\phi)}{d\phi} + \sum_i \frac{dm_i^2(\phi)}{d\phi} \int \frac{d^3\mathbf{p}}{(2\pi)^3 2E_i} f_i(p, x) = 0, \quad (1a)$$

$$\frac{df_i}{dt} = -\mathcal{C}[f], \quad (1b)$$

where $\square = \partial_\mu \partial^\mu$, $f_i(p, x)$ are the particle distribution functions, and $E_i = \sqrt{\mathbf{p}_i^2 + m_i^2}$ the particle energies. $V(\phi)$ is the zero-temperature potential which may include quantum corrections to the classical potential. Considering a bubble wall expanding in the z -direction, and working in the rest frame of the wall where the wall position is taken as $z = 0$, one can obtain the driving and frictional pressures (see, e.g., Ref. [114])

$$\mathcal{P}_{\text{driving}} = V(\phi_s) - V(\phi_b) \equiv \Delta V, \quad (2a)$$

$$\mathcal{P}_{\text{friction}} = - \int_{-\delta}^{\delta} dz (\partial_z \phi) \left(\sum_i \frac{dm_i^2(\phi)}{d\phi} \int \frac{d^3\mathbf{p}}{(2\pi)^3 2E_i} f_i(p, z) \right), \quad (2b)$$

where $\phi_{s,b}$ are the field values at the symmetric and symmetry-broken minima, respectively.² Above, $\delta \gg L_w$ is a length scale. Its value should be chosen such that $|\partial_z \phi / (\Delta\phi)^2|_{\pm\delta} \ll 1$, where $\Delta\phi = \phi_b - \phi_s$. For a wall described by a hyperbolic tangent, one may take, e.g., $\delta = \mathcal{O}(5L_w)$. It can be effectively understood to be infinity in the context of the scalar field EoM.

One can actually use conservation of total energy-momentum to write the frictional pressure in a different way. The energy-momentum tensors for the scalar field and plasma read

$$T_\phi^{\mu\nu} = (\partial^\mu \phi) \partial^\nu \phi - g^{\mu\nu} \left(\frac{1}{2} (\partial\phi)^2 - V(\phi) \right), \quad (3a)$$

$$T_f^{\mu\nu} = (e_f + p_f) u^\mu u^\nu - g^{\mu\nu} p_f, \quad (3b)$$

where u^μ is the fluid four-velocity, and p_f, e_f are the fluid contribution to the pressure and energy density. Note that the perfect fluid form of the plasma energy-momentum tensor already assumes LTE. Since these energy-momentum tensors will be used to derive the two standard matching conditions, we will see how those can be properly interpreted even though the plasma is out-of-equilibrium across the wall. Then

$$\partial_\mu T_\phi^{\mu\nu} = (\partial^\nu \phi) [\square\phi + V'(\phi)] = -(\partial^\nu \phi) \sum_i \frac{dm_i^2(\phi)}{d\phi} \int \frac{d^3\mathbf{p}}{(2\pi)^3 2E_i} f_i(p, x), \quad (4)$$

where in the last equality we have used Eq. (1a). Taking $\nu = z$, using total energy-momentum conservation, and working in the rest frame of the wall, one has

$$\partial_z T_f^{zz} = -(\partial_z \phi) \sum_i \frac{dm_i^2(\phi)}{d\phi} \int \frac{d^3\mathbf{p}}{(2\pi)^3 2E_i} f_i(p, z). \quad (5)$$

²Although generally, FOPT does not necessarily involve symmetry breaking, we will use the terminology of a symmetry-breaking FOPT throughout.

Therefore,

$$\mathcal{P}_{\text{friction}} = \int_{-\delta}^{\delta} dz \partial_z T_f^{zz} = T_f^{zz}|_{\text{in front of the wall}} - T_f^{zz}|_{\text{behind the wall}} \equiv \Delta T_f^{zz}. \quad (6)$$

On the other hand, we know

$$T_f^{zz} = \sum_i \int \frac{d^3\mathbf{p}}{(2\pi)^3} \frac{(p^z)^2}{E_i} f_i(p, z). \quad (7)$$

Once we know f_i obtained from solving the Boltzmann equation, we can substitute them into Eqs. (7), (6) to obtain $\mathcal{P}_{\text{friction}}$ without explicit dependence on ϕ . Note that, in calculating T_f^{zz} , one should only include the degrees of freedom that respond to the passage of the wall quickly enough so that they are not completely “invisible” to the wall. A condition on these degrees of freedom could be that their mean free path should be much smaller than the bubble radius (or the length of the shock wave or rarefaction wave), $L_{\text{MFP}} \ll R_{\text{bubble}}$.

If the interactions among the particles are very efficient, the plasma can remain close to thermal equilibrium during the bubble expansion.³ In such a case, $f_i = f_i^{\text{eq}}$ and one does not need to solve the Boltzmann equation. This is the LTE approximation. This gives the lower bound of the friction on the wall and hence the upper bound of its velocity. On the other hand, if the interactions among the particles are extremely weak, one can take the collision term to be zero in Eq. (1b) and particles in the plasma do not collide with each other while passing through the wall. Again, the Boltzmann equations become very simple and solutions can be obtained straightforwardly. This is the ballistic approximation. These two approximations dramatically simplify the problem but meanwhile, provide the lower and upper bounds on the friction and hence are still very important.

Mathematically, the conditions for the LTE and ballistic approximation to be valid are

$$L_w/\gamma_w \gg L_{\text{MFP}} \propto \frac{1}{\Gamma}, \quad (\text{LTE condition}) \quad (8a)$$

$$L_w/\gamma_w \ll L_{\text{MFP}} \propto \frac{1}{\Gamma}, \quad (\text{ballistic condition}) \quad (8b)$$

where L_w is the wall width *in the wall rest frame*, L_{MFP} is the mean free path *in the plasma frame*, Γ characterizes the collision rate between the particles, and $\gamma_w \equiv 1/\sqrt{1 - v_w^2}$ is the Lorentz boost factor corresponding to v_w . Furthermore, if $L_{\text{MFP}} \ll R_{\text{bubble}}$, which is usually satisfied,⁴ the particles perturbed by the wall’s passage can relax to equilibrium sufficiently fast inside and outside the bubble. Therefore, one can assume a well-defined temperature in front of and behind the wall. We summarise the approximations used in this paper in Table 2.

³Whether the plasma can remain close to LTE also depends on the strength of the force imposed from the wall on the particles.

⁴For example, for an electroweak PT with $T_n \sim 100$ GeV, the mean free path is set by the weak interaction, while $1/(R_{\text{bubble}}H) \sim \beta/H \sim 100$ and the number of relativistic degrees of freedom $g_* \sim 100$. The scales L_{MFP} and the bubble radius at the moment of collision are separated by about 14 orders of magnitude.

Approximation	Scale hierarchy	Reference
LTE	$R_{\text{bubble}} \gg L_w/\gamma_w \gg L_{\text{MFP}}$	[67, 71, 80]
Ballistic (this work)	$R_{\text{bubble}} \gg L_{\text{MFP}} \gg L_w/\gamma_w$	Section 3.2
Ballistic (previous literature)	$L_{\text{MFP}} \gg R_{\text{bubble}} \gg L_w/\gamma_w$	[65, 94]

Table 2: Summary of the different approximations found in the literature and studied in this work, and the scale hierarchies at which they are valid.

There are three ways to apply the ballistic approximation. The first way is commonly considered in the literature [106–112]; one fixes the collision strength and hence L_{MFP} to be the one determined by the model under study, and condition (8b) is satisfied for sufficiently large γ_w . Therefore, the ballistic approximation is used for ultrarelativistic bubble walls, i.e. in the large γ_w limit. This is a faithful application of this approximation, but it only tells us the friction in the ultrarelativistic regime. In the other two approaches, one takes the limit $\Gamma \rightarrow 0$ for given γ_w . In this way, one does not faithfully derive the wall velocity for the considered model but uses the ballistic approximation to derive the upper bound of the friction and thus the lower bound of the wall velocity (the same holds for the use the LTE approximation in this work). In the approach of [65, 94], the plasma temperature and velocity were taken as constant. In this work, on the other hand we also consider inhomogeneous plasma temperature and velocity distributions, thus accounting for hydrodynamic obstruction [68, 75, 80, 105, 114]. We shall observe a higher pressure barrier in the ballistic approximation than in the LTE approximation. This is a crucial observation made in this work.

2.2 The standard matching conditions and fluid equations

Two standard matching conditions To study the matching conditions for the hydrodynamic quantities across the wall, it is convenient to work in the rest frame of the bubble wall (see the right panel of Fig. 1). The matching conditions are usually formulated in terms of the energy density and pressure with the tree-level scalar potential energy absorbed: $e = e_f + V(\phi)$, $p = p_f - V(\phi) \equiv -V_{\text{eff}}(\phi, T)$. Note that the fluid enthalpy is $\omega = e_f + p_f = e + p$. From energy-momentum conservation, we have in equilibrium

$$\omega(z)\gamma^2(z)v(z) = \text{const}, \quad (9a)$$

$$\omega(z)\gamma^2(z)v^2(z) + \frac{1}{2}(\partial_z\phi(z))^2 + p(z) = \text{const}, \quad (9b)$$

where $v > 0$ is defined through $u^\mu = \gamma(1, 0, 0, -v)$ and $\gamma(v) = 1/\sqrt{1-v^2}$. To get the matching conditions, we take $z = \pm\delta'$, (c.f. Table 1). Since the above equations are valid only for LTE (due to the use of the perfect fluid energy-momentum tensor), δ' has to be chosen to be much larger than the mean free path in the wall frame $\gamma_w L_{\text{MFP}}$ (which should really be understood as the mean free path of the particle with the smallest interaction rate). This way, all particles relax to

equilibrium at $\pm\delta'$. On the other hand, δ' should be much smaller than the macroscopic scale so that it can be essentially viewed as infinitesimally thin at the hydrodynamics scale. Therefore, we have $\gamma_w R_{\text{bubble}} \gg \delta' \gg \gamma_w L_{\text{MFP}}$. Then we obtain the following two well-known matching conditions

$$\omega_+ \gamma_+^2 v_+ = \omega_- \gamma_-^2 v_-, \quad (10a)$$

$$\omega_+ \gamma_+^2 v_+^2 + p_+ = \omega_- \gamma_-^2 v_-^2 + p_-, \quad (10b)$$

where a subscript “ \pm ” is used to denote quantities in front of/behind the bubble wall. To be clear, $e_+ = e_s(T_+)$, $e_- = e_b(T_-)$ and similarly for p_{\pm} . Now, the thermodynamic quantities are understood to be the thermal equilibrium ones in the above matching conditions.

Eqs. (10) are definite only when p is a known function of T . This, in principle, requires knowledge about the effective potential of a given model $p = -V_{\text{eff}}(\phi, T)$ where we have included the ϕ -independent term in V_{eff} . We are only interested in the pressures in the symmetric phase $\phi_s(T)$ and the broken phase $\phi_b(T)$, which are determined by minimizing the potential for a given T . Therefore, p can be understood as a function of the temperature only. The other thermodynamic quantities of interest can then be obtained from $p(T)$, e.g.,

$$e = T \frac{dp}{dT} - p, \quad \omega = T \frac{dp}{dT}, \quad s = \frac{\omega}{T}, \quad c^2 = \frac{dp/dT}{de/dT}, \quad (11)$$

where s and c are the entropy density and sound speed respectively. With a known function $p(T)$, Eqs. (10) are two constraint equations for five quantities v_w , T_{\pm} and v_{\pm} . Since T_+ , v_+ can be related to the nucleation temperature T_n and wall velocity v_w , one actually has only one unknown among the five quantities $\{v_w, T_{\pm}, v_{\pm}\}$ after imposing Eqs. (10). In Section 3 we demonstrate how to supplement the system with a third matching condition, such that all quantities are fixed.

To perform a model-agnostic analysis, one usually replaces an exact $p(T)$ with an assumed equation of state (EoS). Often-used examples are the bag EoS or its generalisation, the template model [115]. We briefly review the model-independent analysis of the hydrodynamic matching relations [80] based on the template model in Appendix A, which we also use to provide a proof that the LTE approximation provides a lower bound on the friction in Section 4.1.

Fluid equations Away from the bubble wall ($|z| \sim R_{\text{bubble}} > \delta, \delta'$), the fluid properties are determined by the fluid equations: $u_{\nu} \partial_{\mu} T_f^{\mu\nu} = 0$, $\bar{u}_{\nu} \partial_{\mu} T^{\mu\nu} = 0$, where \bar{u}^{μ} is the normalized vector orthogonal to u^{μ} . For these equations, it is convenient now to work in the rest frame of the bubble center. Then we have $u^{\mu} = \gamma(1, \mathbf{v})$ and $\bar{u}^{\mu} = \gamma(v, \mathbf{v}/v)$. In spherical coordinates, $u^{\mu} = (\gamma, \gamma v, 0, 0)$ and $\bar{u}^{\mu} = (\gamma v, \gamma, 0, 0)$. Since there is no characteristic scale in the problem, the solution should depend only on the dimensionless variable $\xi = r/t$. The fluid equations can be written in a more explicit form, see e.g. Ref. [102].

The fluid dynamics scale is characterised by the bubble radius R_{bubble} while the bubble wall dynamics scale is given by the wall width L_w . The condition $L_w \ll \delta \ll \gamma_w R_{\text{bubble}}$ for Eqs. (2b) and (6) means that although δ can be effectively taken to be infinity in these equations, it can also be effectively viewed as 0^+ in terms of the dimensionless variable ξ in the plasma frame.

Therefore, in ξ -space, one essentially integrates from $\xi_w - 0^+$ to $\xi_w + 0^+$ to obtain the friction. This is reasonable as the friction on the wall only depends on the local state of the plasma near the wall.⁵

3 Bubble wall velocity in the LTE and ballistic approximations

We have just discussed the two well-known hydrodynamic matching relations. Now, we will discuss how we can obtain a third matching relation in the limit of LTE or the ballistic approximation, which allows us to determine v_w .

3.1 The LTE approximation

In the LTE approximation, there is an additional matching condition due to the entropy conservation across the wall [71]

$$\partial_\mu(su^\mu) = 0 \quad \Rightarrow \quad s_+\gamma_+v_+ = s_-\gamma_-v_-, \quad (12)$$

where $s \equiv \partial p / \partial T$ is the entropy density. Using Eq. (10a), it can be also written as

$$\gamma_+T_+ = \gamma_-T_- \quad (\text{LTE matching condition}). \quad (13)$$

This provides the third matching condition as an addition to the previous two given in Eqs. (10a) and (10b). And one can fully determine the wall velocity for any specified effective potential V_{eff} and a given nucleation temperature T_n . In Section 4.1 we present a proof that the LTE limit gives the upper bound on the wall velocity using the template model EoS.

3.2 The ballistic approximation

In the wall frame, a LTE distribution function takes the form

$$f^{\text{eq}}(p^z, z; \mathbf{p}_\perp) = \frac{1}{e^{p_\mu u^\mu / T} \pm 1} = \frac{1}{e^{\beta\gamma(E+vp^z)} \pm 1}, \quad (14)$$

where $\beta \equiv 1/T$, $E = \sqrt{\mathbf{p}^2 + m^2(z)}$. Note that all the quantities except for \mathbf{p} should be understood as a function of z .

In the ballistic approximation, particles *across* the wall are not in LTE. However, one expects that the fluid in front of the wall and behind the wall can have a well-defined temperature for particles moving towards the wall, given by T_+ and T_- , respectively. Furthermore, the bulk velocities of the fluid in front of and behind the wall are given by v_+ , v_- respectively. The incident

⁵In contrast, Refs. [76, 83] define the friction as an integral from $\xi = 0$ to $\xi = 1$ so that the wall friction receives additional contributions from regions far away from the wall.

modes (modes that move towards the wall) are in thermal equilibrium at $z \rightarrow \pm\delta$ (in the rest of this section, we will simply replace δ with ∞ to follow the convention in the literature), i.e.,

$$f_{\infty}^{\leftarrow} = \frac{1}{e^{\beta+\gamma+(E+v+p^z)} \pm 1}, \quad (p^z < 0, z \rightarrow \infty, m = m_+), \quad (15a)$$

$$f_{-\infty}^{\rightarrow} = \frac{1}{e^{\beta-\gamma-(E+v-p^z)} \pm 1}, \quad (p^z > 0, z \rightarrow -\infty, m = m_- > m_+), \quad (15b)$$

where we have denoted $m_{\pm} = m(z \rightarrow \pm\infty)$. Above and in the following, we assume that the particles gain mass when they enter the bubble. In Appendix C, we extend the analysis to the case when particles lose mass as they enter the bubble.

The full distribution should be determined by the Liouville equation

$$\left(\frac{p^z}{E} \partial_z - \frac{\partial_z m^2}{2E} \partial_{p^z} \right) f(p^z, z; \mathbf{p}_{\perp}) = 0. \quad (16)$$

Using $\partial_z = (\partial_z m^2) \partial_{m^2}$, one has

$$\frac{p^z (\partial_z m^2)}{E} (\partial_{m^2} - \partial_{p^{z2}}) f(p^z, z; \mathbf{p}_{\perp}) = 0. \quad (17)$$

This simply means that f is a function of the combination $m^2 + p^{z2}$. As a consequence, it should be straightforward to obtain the solution for a given boundary condition.

The solution to the Liouville equation with the boundary conditions (15) can be interpreted physically [65, 94].

(1) Transmission from the symmetric phase (t_+):

$$f^{t+}(p^z, z; \mathbf{p}_{\perp}) = \frac{1}{e^{\beta+\gamma+(E-v+\sqrt{p^{z2}+m^2(z)-m_+^2})} \pm 1}, \quad \left(p^z < -\sqrt{m_-^2 - m^2(z)} \right); \quad (18)$$

(2) Reflection (r):

$$f^r(p^z, z; \mathbf{p}_{\perp}) = \frac{1}{e^{\beta+\gamma+(E-v+\sqrt{p^{z2}+m^2(z)-m_+^2})} \pm 1}, \quad \left(-\sqrt{m_-^2 - m^2(z)} < p^z < \sqrt{m_-^2 - m^2(z)} \right); \quad (19)$$

Note that above we do not have $\sqrt{p^{z2} + m^2(z) - m_+^2}$ multiplied with a factor of $\text{sign}[p^z]$, in contrast to Ref. [65].⁶

⁶This observation has also been made in Ref. [88]. However, our solutions differ from those given in Ref. [88]. We have taken into account the inhomogeneity in the fluid velocity so that v_+ , v_- enter the solutions. There seem to be also some sign differences between our solutions and those in Ref. [88].

(3) Transmission from inside the bubble (t_-):

$$f^{t-}(p^z, z; \mathbf{p}_\perp) = \frac{1}{e^{\beta-\gamma_-(E+v_-\sqrt{p^{z2}+m^2(z)-m^2})} \pm 1}, \quad \left(p^z > \sqrt{m_-^2 - m^2(z)}\right). \quad (20)$$

The above solution completes the distribution function for all the p^z -modes in front of the wall ($z \rightarrow \infty$) and behind the wall ($z \rightarrow -\infty$). Explicitly, at $z \rightarrow \infty$, we have

$$f(p^z, \infty; \mathbf{p}_\perp) = \begin{cases} \frac{1}{e^{\beta+\gamma_+(E+v_+p^z)} \pm 1}, & p^z < -\sqrt{\Delta m^2}, & (t^+\text{-modes}) \\ \frac{1}{e^{\beta+\gamma_+(E-v_+|p^z|)} \pm 1}, & -\sqrt{\Delta m^2} < p^z < \sqrt{\Delta m^2}, & (r\text{-modes}) \\ \frac{1}{e^{\beta-\gamma_-(E+v_-\sqrt{p^{z2}-\Delta m^2})} \pm 1}, & p^z > \sqrt{\Delta m^2}, & (t^-\text{-modes}) \end{cases}, \quad (21)$$

where $\Delta m^2 \equiv m_-^2 - m_+^2$. In general Δm^2 is not equal to $(\Delta m)^2 \equiv (m_- - m_+)^2$ unless $m_+ = 0$. At $z \rightarrow -\infty$, we have

$$f(p^z, -\infty; \mathbf{p}_\perp) = \begin{cases} \frac{1}{e^{\beta+\gamma_+(E-v_+\sqrt{p^{z2}+\Delta m^2})} \pm 1}, & p^z < 0, & (t^+\text{-modes}) \\ \frac{1}{e^{\beta-\gamma_-(E+v_+p^z)} \pm 1}, & p^z > 0, & (t^-\text{-modes}) \end{cases}. \quad (22)$$

Note that behind the wall, there are no r -modes. This is reasonable as reflected particles do not enter the wall. We also note that T_+, T_- are not defined for all the modes in front of/behind the wall. Let us stress that there is an important difference between the approach we take and the ballistic computation done in [65, 94]; we distinguish the fluid velocity and temperature in front of and behind the bubble wall, whereas in [65, 94], these are taken to be constant at v_w and T_n respectively. As we will see explicitly in Sec. 5.2, this has a significant effect on the pressure, especially at velocities close to the Jouguet velocity (the transition from hybrid solutions to detonations). With the assumption of a constant fluid velocity and temperature, the ballistic approximation does *not* provide an upper bound on the friction. On the other hand, the ballistic approximation studied here is the limit one would obtain when solving the Boltzmann equation and slowly turning off the collisions in the plasma ($\mathcal{C}[f] \rightarrow 0$) which as we will show, makes it indeed the upper bound on the friction and thus lower bound on the wall velocity.

To compute the pressure on the wall, it is convenient to isolate the contribution from each mode. Using Eqs. (6) and (7), one can then write

$$\mathcal{P}_{\text{friction}}^b(T_+, T_-, v_+, v_-) = \mathcal{P}^{t+} + \mathcal{P}^{t-} + \mathcal{P}^r, \quad (23)$$

with

$$\mathcal{P}^{t+} = \int_{p^z < -\sqrt{\Delta m^2}} \frac{d^3 \mathbf{p}}{(2\pi)^3} \frac{(p^z)^2}{E_+} f^{t+}(p^z, +\infty) - \int_{p^z < 0} \frac{d^3 \mathbf{p}}{(2\pi)^3} \frac{(p^z)^2}{E_-} f^{t+}(p^z, -\infty), \quad (24a)$$

$$\mathcal{P}^{t-} = \int_{p^z > \sqrt{\Delta m^2}} \frac{d^3 \mathbf{p}}{(2\pi)^3} \frac{(p^z)^2}{E_+} f^{t-}(p^z, +\infty) - \int_{p^z > 0} \frac{d^3 \mathbf{p}}{(2\pi)^3} \frac{(p^z)^2}{E_-} f^{t-}(p^z, -\infty), \quad (24b)$$

$$\mathcal{P}^r = \int_{|p^z| < \sqrt{\Delta m^2}} \frac{d^3 \mathbf{p}}{(2\pi)^3} \frac{(p^z)^2}{E_+} f^r(p^z, +\infty), \quad (24c)$$

where $E_{\pm} = E(z = \pm\infty)$ and we did not make the \mathbf{p}_{\perp} -dependence in the distribution functions explicit. These equations can be simplified by observing that

$$f^{t+}(p^z, +\infty) = f^{\text{eq}}(p^z, +\infty), \quad f^{t-}(p^z, -\infty) = f^{\text{eq}}(p^z, -\infty), \quad (25a)$$

$$f^{t+}(p^z, -\infty) = f^{\text{eq}}(-\sqrt{p^{z2} + \Delta m^2}, +\infty), \quad f^{t-}(p^z, +\infty) = f^{\text{eq}}(+\sqrt{p^{z2} - \Delta m^2}, -\infty) \quad (25b)$$

and $f^r(p^z, +\infty) = f^{\text{eq}}(-|p^z|, +\infty)$ to replace all the ballistic distribution functions with the corresponding equilibrium one. Then, with appropriate changes of variables, the pressures can be written as

$$\mathcal{P}^{t+} = \int_{p^z < -\sqrt{\Delta m^2}} \frac{d^3\mathbf{p}}{(2\pi)^3} \frac{p^z}{E_+} \left(p^z + \sqrt{(p^z)^2 - \Delta m^2} \right) f^{\text{eq}}(p^z, +\infty), \quad (26a)$$

$$\mathcal{P}^{t-} = \int_{p^z > 0} \frac{d^3\mathbf{p}}{(2\pi)^3} \frac{p^z}{E_-} \left(\sqrt{(p^z)^2 + \Delta m^2} - p^z \right) f^{\text{eq}}(p^z, -\infty), \quad (26b)$$

$$\mathcal{P}^r = 2 \int_{-\sqrt{\Delta m^2} < p^z < 0} \frac{d^3\mathbf{p}}{(2\pi)^3} \frac{(p^z)^2}{E_+} f^{\text{eq}}(p^z, +\infty). \quad (26c)$$

The total frictional pressure in the ballistic approximation finally takes the simple form

$$\mathcal{P}_{\text{friction}}^b = \int \frac{d^3\mathbf{p}}{(2\pi)^3} \frac{p^z}{E} \Delta p^z f^{\text{eq}}, \quad (27)$$

where Δp^z is the exchanged momentum with the wall and f^{eq} and E are evaluated at $z \rightarrow +\infty$ for r and t^+ modes and $z \rightarrow -\infty$ for the t^- mode. This last equation has a clear physical interpretation: particles coming from $\pm\infty$ hit the wall with a flux $\frac{p^z}{E_{\pm}} f^{\text{eq}}(p^z, \pm\infty)$ with each collision transferring the momentum Δp^z to the wall. The final friction felt by the wall is then obtained by integrating the product of these two factors.

The integrals simplify if we approximate the Bose-Einstein/Fermi-Dirac distribution by the Boltzmann distribution. Integrating over \mathbf{p}_{\perp} analytically and with appropriate changes of variables, we obtain

$$\mathcal{P}^{t+} = \frac{T_+^4}{4\pi^2\gamma_+} \int_{x > \sqrt{\Delta m^2}/T_+} dx x \left(x - \sqrt{x^2 - \Delta m^2/T_+^2} \right) e^{-\gamma_+(\sqrt{x^2 + m_+^2/T_+^2} - v_+ x)}, \quad (28a)$$

$$\mathcal{P}^{t-} = \frac{T_-^4}{4\pi^2\gamma_-} \int_{x > 0} dx x \left(\sqrt{x^2 + \Delta m^2/T_-^2} - x \right) e^{-\gamma_-(\sqrt{x^2 + m_-^2/T_-^2} + v_- x)}, \quad (28b)$$

$$\mathcal{P}^r = \frac{T_+^4}{2\pi^2\gamma_+} \int_{0 < x < \sqrt{\Delta m^2}/T_+} dx x^2 e^{-\gamma_+(\sqrt{x^2 + m_+^2/T_+^2} - v_+ x)}. \quad (28c)$$

We present the corresponding expressions of the various pressures for Bose-Einstein and Fermi-Dirac distributions in Appendix B.

At last,

$$\Delta V = \mathcal{P}_{\text{friction}}^{\text{b}}(T_+, T_-, v_+, v_-) \quad (\text{ballistic matching condition}) \quad (29)$$

effectively provides an additional matching condition for $\{T_+, T_-, v_+, v_-\}$ and hence we can solve the wall velocity as we do for the LTE case. In reality, there are typically multiple particle species that couple with the order-parameter scalar ϕ . In that case, one needs to sum over all the contributions with parameters $m_{i,\pm}$.

The relativistic-detonation limit As mentioned earlier, the ballistic condition (8b) itself does not necessarily require ultrarelativistic walls. However, it is interesting to see how the standard Bökder-Moore 1-to-1 thermal friction, derived in the $\gamma_w \rightarrow \infty$ limit [106], can be recovered from the above formulae. In the limit $\gamma_w \rightarrow \infty$, the equilibrium distribution function (14) is a very narrow distribution peaked at $p^z = -\gamma T$ (see e.g. [112]). Therefore, from the integral ranges in Eqs. (26), one sees that \mathcal{P}^{t-} and \mathcal{P}^r are suppressed compared with \mathcal{P}^{t+} . Furthermore, for $\gamma_w \rightarrow \infty$, one can well assume that the bubble motion is in the detonation mode and thus f^{eq} in front of the wall is estimated at the nucleation temperature $T_+ = T_n$. Since only the narrow region near $-\gamma_w T_n$ makes the dominant contribution to the integral of \mathcal{P}^{t+} , one can Taylor expand $\sqrt{p^{z2} - \Delta m^2} \approx p^z - \frac{\Delta m^2}{2p^z}$, assuming $|p^z| \gg \Delta m^2$. Finally one gets

$$\begin{aligned} \mathcal{P}_{\gamma_w \rightarrow \infty} &\approx \mathcal{P}^{t+} \approx \Delta m^2 \int_{p^z < -\Delta m} \frac{d^3 \mathbf{p}}{(2\pi)^3 2E_+} f^{\text{eq}}(p^z, +\infty; T_n) \\ &\approx \Delta m^2 \int \frac{d^3 \mathbf{p}}{(2\pi)^3 2E_+} f^{\text{eq}}(p^z, +\infty; T_n) \end{aligned} \quad (30)$$

$$\stackrel{m_{\pm}=0}{=} \begin{cases} \Delta m^2 T^2 / 48, & \text{fermions} \\ \Delta m^2 T^2 / 24, & \text{bosons} \end{cases} \quad (31)$$

where the last expression is the standard Bökder-Moore 1-to-1 thermal friction \mathcal{P}_{BM} which is valid when $m_+ = 0$.

4 Demonstration that LTE and ballistic provide bounds on the wall velocity

Having discussed how the LTE and ballistic approximations simplify the computation of the bubble wall velocity, here we demonstrate that they indeed provide bounds on the wall velocity and friction. We will first prove that the LTE gives an upper bound of the wall velocity using the template model (cf. Appendix A), following Ref. [114]. Then, we give a more general argument based on the linearized Boltzmann equation.

4.1 LTE as upper bound on the wall velocity in the template model

In the general case where LTE is not maintained in the plasma, one cannot expect entropy to be conserved across the wall. Therefore, Eq. (12) must be replaced by the more general condition

of the non-negativity of entropy production [116]

$$v_- \gamma_- s_- - v_+ \gamma_+ s_+ = v_+ \gamma_+ \Delta s \geq 0. \quad (32)$$

Here, Δs quantifies the variation of entropy which depends on the deviation from equilibrium across the wall, making it a highly model-dependent quantity. Nevertheless, as the total entropy cannot decrease, Δs is always positive, and this fact can be used to prove that the LTE limit gives an upper bound of the wall velocity. We will restrict our proof to the template EoS.

Using Eq. (32) instead of (12), the temperature behind the wall can now be expressed as

$$T_- = \frac{\gamma_+ T_+}{\gamma_- (1 + \sigma)}, \quad (33)$$

where we have defined

$$\sigma \equiv \Delta s / s_+ \geq 0. \quad (34)$$

Substituting the above into Eq. (A77a) to remove the dependence on T_- , one finally obtains

$$3\nu\alpha_+ v_+ v_- = \left[1 - 3\alpha_+ - \left(\frac{\gamma_+}{\gamma_-} \right)^\nu \frac{\Psi_+}{(1 + \sigma)^\nu} \right] \left(1 - \frac{v_+ v_-}{c_b^2} \right), \quad (35)$$

where the corresponding quantities are defined in Appendix A. The above equation is the same as the LTE matching equation (A78) with the simple substitution

$$\Psi \rightarrow \Psi_{\text{eff}} = \frac{\Psi}{(1 + \sigma)^\nu} \leq \Psi, \quad (36)$$

where the last inequality comes from $\sigma \geq 0$.

We conclude that, within the hydrodynamic description, an out-of-equilibrium plasma can be treated mathematically like an LTE plasma, with an effective Ψ_{eff} which gets reduced compared with the physical Ψ by the entropy production. Note that this is just a mathematical correspondence. In the presence of a deviation from LTE, Ψ_{eff} loses the original meaning as the ratio of the enthalpies in the broken and symmetric phases. In LTE, a smaller value of Ψ leads to a smaller wall velocity (see Ref. [80]), as it means more particles can interact with the wall leading to a higher friction force. Using the correspondence above, this means that entropy production typically makes the wall velocity smaller compared with the limit of no entropy production. Hence the LTE approximation ($\sigma = 0$) gives the upper bound of the wall velocity.

Interestingly, in the limit $\Psi \rightarrow 0$ where all the degrees of freedom become very massive and cannot enter the bubble wall, one can see that LTE always gives an exact result as $\Psi_{\text{eff}} = \Psi = 0$. This curious fact was already pointed out in Ref. [85] and happens because in this limit, there is no plasma on the broken side which implies $s_- = 0$. With that constraint, it is easy to see that the only non-negative value Eq. (32) can have is 0. Therefore, entropy must be conserved and LTE becomes exact.

4.2 Demonstration that LTE and ballistic approximations bound v_w in the linearized Boltzmann equation

The general Boltzmann equation for the deviation from equilibrium $\delta f = f - f^{\text{eq}}$ of a single particle can be written as

$$\left(p^z \partial_z - \frac{1}{2} \partial_z(m^2) \partial_{p^z}\right) \delta f + \lambda \mathcal{C}[\delta f](z, p^z) = - \left(p^z \partial_z - \frac{1}{2} \partial_z(m^2) \partial_{p^z}\right) f^{\text{eq}} \equiv S(z, p^z), \quad (37)$$

where the parameter λ represents the strength of the interactions involved in the collisions.⁷ The ballistic limit can be obtained by taking $\lambda \rightarrow 0$, while LTE is obtained in the limit $\lambda \rightarrow \infty$. In general, $\mathcal{C}[\delta f](z, p^z)$ is a nonlinear functional of δf (which is ultimately a function of z and p^z), but for simplicity, we will linearize it with respect to δf . We will also assume $\partial_z(m^2) < 0$, such that the particle becomes heavier when entering the bubble.

This equation can be simplified with the change of variable $\rho = \sqrt{(p^z)^2 + m^2}$, which leads to the equation

$$\text{sign}(p^z) \sqrt{\rho^2 - m^2} \frac{d}{dz} \delta f(z) + \lambda \mathcal{C}[\delta f] \left(z, \text{sign}(p^z) \sqrt{\rho^2 - m^2} \right) = S \left(z, \text{sign}(p^z) \sqrt{\rho^2 - m^2} \right), \quad (38)$$

where $\delta f(z) = \delta f(z, \text{sign}(p^z) \sqrt{\rho^2 - m^2}(z))$. We thus see that in terms of the ρ variable, the modes with positive and negative momentum are governed by two distinct Boltzmann equations. This can be written in a simpler form as

$$\frac{d}{dz} \delta f(z) - \lambda \mathcal{H}[\delta f](z, \rho, \text{sign}(p^z)) = \mathcal{S}(z, \rho, \text{sign}(p^z)), \quad (39)$$

with

$$\begin{aligned} \mathcal{H}[\cdot](z, \rho, \text{sign}(p^z)) &= - \frac{\text{sign}(p^z)}{\sqrt{\rho^2 - m^2}} \mathcal{C}[\cdot] \left(z, \text{sign}(p^z) \sqrt{\rho^2 - m^2} \right), \\ \mathcal{S}(z, \rho, \text{sign}(p^z)) &= \frac{\text{sign}(p^z)}{\sqrt{\rho^2 - m^2}} S \left(z, \text{sign}(p^z) \sqrt{\rho^2 - m^2} \right) = - \frac{d}{dz} f^{\text{eq}}(z). \end{aligned} \quad (40)$$

To continue, it will be convenient to represent functions of ρ and $\text{sign}(p^z)$ as states of a vectorial space \mathcal{V} . The solution $\delta f(z, \rho, \text{sign}(p^z))$ is now represented by a state $|\delta f(z)\rangle \in \mathcal{V}$, and similarly $\mathcal{S}(z, \rho, \text{sign}(p^z)) \rightarrow |\mathcal{S}(z)\rangle \in \mathcal{V}$. The parameter z here is analogous to the time parameter in the Schrödinger equation. Finally, the functional $\mathcal{H}[\cdot](z, \rho, \text{sign}(p^z))$ is now represented by a map $\mathcal{H}(z)$ from \mathcal{V} to \mathcal{V} .

The Boltzmann equations can then be expressed as

$$\frac{d}{dz} |\delta f(z)\rangle - \lambda \mathcal{H}(z) |\delta f(z)\rangle = |\mathcal{S}(z)\rangle. \quad (41)$$

⁷Note that λ does not correspond to a physical quantity and should be set to 1 in a calculation. We introduce it here to study the variation of the solution with respect to the collision strength and to take the different limits.

To solve this equation, it will be useful to define the projection operators \mathcal{P}_\pm that project out the negative and positive eigenvalues of \mathcal{H} . In other words, $\mathcal{H}_+ \equiv \mathcal{P}_+ \mathcal{H} = \mathcal{H} \mathcal{P}_+$ is positive definite and $\mathcal{H}_- \equiv \mathcal{P}_- \mathcal{H} = \mathcal{H} \mathcal{P}_-$ is negative definite. They also satisfy $\mathcal{P}_\pm^2 = \mathcal{P}_\pm$, $\mathcal{P}_+ \mathcal{P}_- = 0$, and since \mathcal{H} has no zero eigenvalues,⁸ $\mathcal{P}_+ + \mathcal{P}_- = \mathbf{1}$. Applying these operators on Eq. (41), the positive and negative eigenmodes decouple as

$$\frac{d}{dz} |\delta f_\pm(z)\rangle - \lambda \mathcal{H}_\pm(z) |\delta f_\pm(z)\rangle = |\mathcal{S}_\pm(z)\rangle, \quad (42)$$

where $|\delta f_\pm\rangle = \mathcal{P}_\pm |\delta f\rangle$ and $|\mathcal{S}_\pm\rangle = \mathcal{P}_\pm |\mathcal{S}\rangle$. Physically, $|\delta f_\pm\rangle$ are deviations from equilibrium generated by particles coming from $\pm\infty$, respectively.

Let us now define the evolution operators $U_\pm(z, z')$ in terms of Dyson series as

$$\begin{aligned} U_\pm(z, z') &= \mathcal{T} \exp \left(\lambda \int_{z'}^z dy \mathcal{H}_\pm(y) \right) \\ &= \sum_{n=0}^{\infty} \frac{1}{n!} \mathcal{T} \left(\lambda \int_{z'}^z dy \mathcal{H}_\pm(y) \right)^n \\ &= \mathbf{1} + \lambda \int_{z'}^z dy \mathcal{H}_\pm(y) + \lambda^2 \int_{z'}^z dy \int_{z'}^y dy' \mathcal{H}_\pm(y) \mathcal{H}_\pm(y') + \dots, \end{aligned} \quad (43)$$

where \mathcal{T} is the time-ordering operator (or position-ordering here), which arranges the \mathcal{H}_\pm operators following it in order of decreasing distance from z' , such that the one most on the left is evaluated at the point farthest from z' , and the one on the right is evaluated at the point closest to z' . The evolution operators have the important properties that $U_\pm(z, z) = \mathbf{1}$ and that their derivative with respect to z is

$$\partial_z U_\pm(z, z') = \lambda \mathcal{H}_\pm(z) + \lambda^2 \mathcal{H}_\pm(z) \int_{z'}^z dy \mathcal{H}_\pm(y) + \dots = \lambda \mathcal{H}_\pm(z) U_\pm(z, z'). \quad (44)$$

Using these properties, it becomes straightforward to show that the solutions of Eqs. (42) are

$$|\delta f_+(z)\rangle = - \int_z^\infty dz' U_+(z, z') |\mathcal{S}_+(z')\rangle, \quad (45a)$$

$$|\delta f_-(z)\rangle = \int_{-\infty}^z dz' U_-(z, z') |\mathcal{S}_-(z')\rangle. \quad (45b)$$

Notice that the U_\pm appearing in these solutions are both exponentials of negative definite operators, which guarantees that U_\pm are positive definite and that the integrals converge (because $U_\pm(z, \mp\infty) = U_\pm(\pm\infty, z) = 0$). Finally, the complete solution of the Boltzmann equation (41) is

$$|\delta f(z)\rangle = |\delta f_+(z)\rangle + |\delta f_-(z)\rangle = - \int_z^\infty dz' U_+(z, z') |\mathcal{S}_+(z')\rangle + \int_{-\infty}^z dz' U_-(z, z') |\mathcal{S}_-(z')\rangle. \quad (46)$$

⁸The nonlinear collision operator *does* have zero eigenvalues, as it must satisfy $\mathcal{C}|f^{\text{eq}}\rangle = 0$. After linearising this operator, this equation becomes $\mathcal{C}^{\text{linear}}|\delta f = 0\rangle = 0$. However, a zero state cannot be an eigenstate. Furthermore, zero eigenvalues lead to divergent solutions (see Eqs. (45)), hence cannot exist.

We now wish to demonstrate how $|\delta f(z)\rangle$ varies with the interaction's strength, parametrized by λ . It is straightforward to show that the derivative of the evolution operators with respect to λ is

$$\frac{\partial}{\partial \lambda} U_{\pm}(z, z') = \int_{z'}^z dy \mathcal{T} [\mathcal{H}_{\pm}(y) U_{\pm}(z, z')]. \quad (47)$$

Note that, from the definition of the time-ordering operator \mathcal{T} , one has the relation $\mathcal{T}[\mathcal{H}_{\pm}(z), \mathcal{H}_{\pm}(z')] = 0$. This implies the property $U_{\pm}(z, z'') = U_{\pm}(z, z') U_{\pm}(z', z'')$. Using this relation, the variation of the solutions with respect to λ is

$$\begin{aligned} \frac{\partial}{\partial \lambda} |\delta f_+(z)\rangle &= - \int_z^{\infty} dz' \int_{z'}^z dy \mathcal{T} [\mathcal{H}_+(y) U_+(z, z')] |\mathcal{S}_+(z')\rangle \\ &= - \int_z^{\infty} dz' \left\{ -\partial_{z'} \left[\int_{z'}^z dy \int_{z'}^{\infty} dy' \mathcal{T} [\mathcal{H}_+(y) U_+(z, y')] |\mathcal{S}_+(y')\rangle \right] \right. \\ &\quad \left. - \int_{z'}^{\infty} dy' \mathcal{T} [\mathcal{H}_+(z') U_+(z, y')] |\mathcal{S}_+(y')\rangle \right\} \\ &= \int_z^{\infty} dz' \int_{z'}^{\infty} dy' U_+(z, z') \mathcal{H}_+(z') U_+(z', y') |\mathcal{S}_+(y')\rangle \\ &= - \int_z^{\infty} dz' U_+(z, z') \mathcal{H}_+(z') |\delta f_+(z')\rangle, \end{aligned} \quad (48)$$

where the first term of the second line is zero because it is a total derivative vanishing at the boundaries, and we used Eq. (45a) to get the fourth line. Similarly, we get

$$\frac{\partial}{\partial \lambda} |\delta f_-(z)\rangle = \int_{-\infty}^z dz' U_-(z, z') \mathcal{H}_-(z') |\delta f_-(z')\rangle. \quad (49)$$

These last two equations can be combined as

$$\frac{\partial}{\partial \lambda} |\delta f(z)\rangle = - \int_{-\infty}^{\infty} dz' |U(z, z') \mathcal{H}(z')| |\delta f(z')\rangle, \quad (50)$$

with $|U(z, z') \mathcal{H}(z')| = U_+(z, z') \mathcal{H}_+(z') \Theta(z' - z) - U_-(z, z') \mathcal{H}_-(z') \Theta(z - z')$, which is a positive definite operator.

Going back to the representation in terms of functions of ρ and $\text{sign}(p^z)$, $|U\mathcal{H}|$ becomes a functional which, due to its positive definiteness, maps every positive function to another positive function and vice versa. Therefore, Eq. (50) implies that as we increase λ , the solution becomes closer and closer to zero, which corresponds to equilibrium.

However, in general, the solution of the Boltzmann equation δf is not positive for all values of z, p^z . In fact, because U_{\pm} are positive definite operators and because $\mathcal{S} = -df^{\text{eq}}/dz < 0$ (the particle is more massive in the bubble at $z \rightarrow -\infty$ and therefore Boltzmann suppressed), one can see from Eqs. (45) that $\delta f_+ > 0$ and $\delta f_- < 0$. In practice, the pressure on the wall is dominated by the contribution from δf_+ , as it corresponds to particles coming from the symmetric phase that are either transmitted to the broken phase or reflected, while δf_- contains particles transmitted from the broken to the symmetric phases. The latter are typically Boltzmann suppressed since

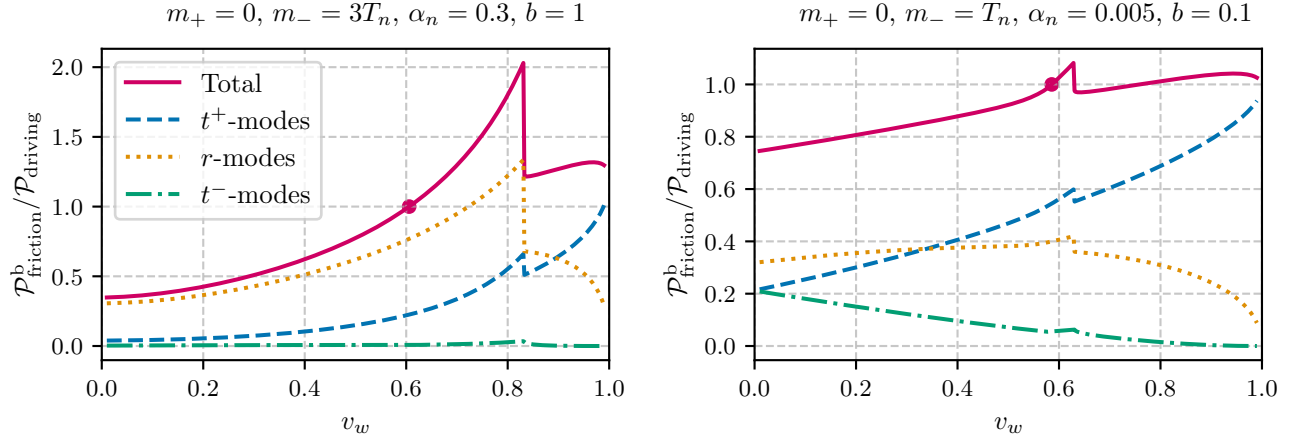


Figure 2: Different contributions to the ballistic pressure for a strong (left) and a weak (right) PT in the model presented in Section 5.1. In both cases, the t^- -modes (which correspond to δf_+) give the smallest contribution. The points show the solutions satisfying $\mathcal{P}_{\text{friction}}^b / \mathcal{P}_{\text{driving}} = 1$.

they are created in a phase where they are more massive. Also, to interact with the wall, they need to be faster than v_w to catch up with it, which only a small fraction of the particles can do (intuitively, we expect this fraction to go from $1/2$ at $v_w = 0$ to 0 at $v_w = 1$). It is therefore a good approximation to neglect δf_- in the pressure calculation and set $\delta f \approx \delta f_+$. This fact can be seen explicitly in Fig. 2 which shows the contribution of the different modes to the ballistic pressure. In both the strong and weak PTs, the t^- -modes (which correspond to δf_-) give the smallest contribution, and they are completely negligible in the strong PT.

From Eqs. (45) and (49), one finally gets $\delta f > 0$ and $\partial_\lambda \delta f < 0$. From Eq. (2b), one has

$$\mathcal{P}_{\text{friction}} = \mathcal{P}_{\text{LTE}} - \sum_i \int_{-\delta}^{\delta} dz \underbrace{\frac{dm_i^2(\phi(z))}{dz}}_{<0} \underbrace{\left(\int \frac{d^3\mathbf{p}}{(2\pi)^3 2E_i} \delta f_i \right)}_{>0}, \quad (51)$$

where \mathcal{P}_{LTE} is obtained by substituting $f_i = f_i^{\text{eq}}$ into Eq. (2b). $\delta f_i > 0$ means that out-of-equilibrium effects add more friction compared with the LTE limit. While $\partial_\lambda \delta f_i < 0$ means that the minimum is reached when $\lambda \rightarrow \infty$ (LTE) and the maximum pressure is reached when $\lambda = 0$ (ballistic limit).

5 Comparison between LTE and ballistic results

As the LTE and ballistic approximations respectively offer an upper and lower bound on the true wall velocity, it can be useful to compare these two approximations to find constraints on the wall velocity without having to solve a complicated system of Boltzmann equations and scalar EoM. Not only are these equations challenging and computationally expensive to solve, they also suffer from large theoretical uncertainties coming from the collision rates Γ that appear in the Boltzmann equations. These collision rates are typically computed to leading-log accuracy, which is rather imprecise and can lead to errors of $\mathcal{O}(1)$ [68, 75, 92, 117].

The LTE and ballistic approximations allow us to avoid this problem since they correspond to the limits $\Gamma \rightarrow \infty$ and $\Gamma \rightarrow 0$, respectively. Thus, even if Γ is completely unknown, one can still obtain useful information on v_w with these approximations in the form of an interval in which it must reside.

Unfortunately, making a general comparison between LTE and ballistic is not a straightforward task as these two approximations depend on a different set of variables. In general, this mapping from one approximation to the other cannot be made in a model-independent way. It either necessitates specifying a model, in which case the mapping can be done exactly, or making approximations which allows one to make more general conclusions that should still hold at least qualitatively. We will explore both options in the following.

5.1 Model-independent analysis

To obtain a more general and qualitative understanding of how the LTE and ballistic approximation compare to one another, we now study a set of simplified models. We will assume that the plasma contains \tilde{g}_\star massless degrees of freedom and $g_{\star,\phi}$ degrees of freedom with a mass of m_+ and m_- outside and inside the bubble, respectively. The pressure in this model can therefore be expressed as

$$p_{s/b}(T) = \frac{\pi^2 \tilde{g}_\star}{90} T^4 + g_{\star,\phi} p_{M,s/b}(T) - \epsilon_\pm, \quad (52)$$

where ϵ_\pm is the vacuum contribution (which is approximated to be independent of T), and $p_{M,s/b}$ is the thermal pressure of a single degree of freedom with mass m_\pm . To simplify the discussion, we will assume that $p_{M,s/b}$ is given by the one-loop Maxwell-Boltzmann pressure, which is given by

$$p_{M,s/b}(T) = \frac{\pi^4 m_\pm^2 T^2}{90 \cdot 2\pi^2} K_2\left(\frac{m_\pm}{T}\right), \quad (53)$$

where $K_n(x)$ is the modified Bessel function of the second kind. Above, we have added by hand an extra factor $\pi^4/90 \approx 1.08$ so that p_M reproduces the value of the Bose-Einstein distribution for $m_\pm = 0$. This way, $g_{\star,\phi}$ can be taken to be the effective number of degrees of freedom coupling with the scalar ϕ ,

$$g_{\star,\phi} = \sum_{i_B} g_{i_B,\phi} + \sum_{i_F} \frac{7}{8} g_{i_F,\phi}, \quad (54)$$

where $g_{i_B,\phi}$ is the number of internal degrees of freedom of boson i_B , and $g_{i_F,\phi}$ of fermion i_F . When $m_\pm = 0$, the total number of relativistic degrees of freedom in the symmetric phase is $\tilde{g}_\star + g_{\star,\phi} \equiv g_\star$.

It follows directly that the enthalpy and energy densities are given by

$$\omega_{s/b}(T) = \frac{2\pi^2 \tilde{g}_\star}{45} T^4 + g_{\star,\phi} \frac{\pi^4 m_\pm^3 T}{90 \cdot 2\pi^2} K_3\left(\frac{m_\pm}{T}\right), \quad (55a)$$

$$e_{s/b}(T) = \frac{\pi^2 \tilde{g}_\star}{30} T^4 + g_{\star,\phi} \frac{\pi^4 m_\pm^2 T}{90 \cdot 2\pi^2} \left[m_\pm K_3\left(\frac{m_\pm}{T}\right) - T K_2\left(\frac{m_\pm}{T}\right) \right] + \epsilon_\pm. \quad (55b)$$

At first sight, it could appear that the EoS (52) depends on six parameters (\tilde{g}_* , $g_{*,\phi}$, m_{\pm} and ϵ_{\pm}). However, one can see that the variables \tilde{g}_* , $g_{*,\phi}$ and ϵ_{\pm} only appear in the combinations

$$b = \frac{g_{*,\phi}}{\tilde{g}_*}, \quad \epsilon = \frac{\epsilon_+ - \epsilon_-}{\tilde{g}_*}, \quad (56)$$

in all the matching equations. This effectively lowers the number of independent variables in this model to four.

Finally, to simplify the LTE calculation, one can map the EoS (52) to the template model (see Appendix A) by computing the thermodynamic quantities $\alpha(T_n)$, $c_{s/b}(T_n)$ and $\Psi(T_n)$ with Eqs. (A76), (11) and (A79). This typically gives a reasonable approximation and allows one to use the method presented in Ref. [80] to compute v_w . However, to guarantee accurate results, we will keep the full EoS (52) in what follows and use the `WallGo` package [91] to find the LTE wall velocity (based on hydrodynamics [71]).

5.1.1 Results

We now move to comparing the wall velocity obtained within this model using the ballistic and LTE limits. As argued previously, these limits give respectively a lower and upper bound on the possible wall velocities and can therefore contain helpful information. We will be particularly interested in the difference between these two predictions. If the difference is large (or if they predict different types of solutions), the true wall velocity remains poorly constrained and it is required to solve a set of Boltzmann equations to obtain a better estimate. On the other hand, if the difference is small, the collision operator has very little effect on the wall velocity and it may be unnecessary to solve the Boltzmann equations.

In what follows, it will be convenient to describe the strength of the PT with a slightly different definition of α than the one defined in terms of the pseudo trace $\bar{\theta}$ (see Eq. (A76)). Instead, we will use a definition based on the pressure difference:

$$\alpha_p(T) = -(1 + 1/c_b^2) \left(\frac{p_s(T) - p_b(T)}{3\omega_s(T)} \right) = \alpha(T) - \frac{1 - \Psi(T)}{3}. \quad (57)$$

The two definitions are approximately equal for strong PTs, but slightly disagree for weaker ones. In particular, by definition, α_p vanishes when $\Delta V = 0$, so it can always take values from 0 to ∞ , while α cannot be smaller than $(1 - \Psi)/3$. Furthermore, the wall velocity always goes to 0 in the limit $\alpha_p \rightarrow 0$. These properties make it easier to interpret and present results expressed in terms of α_p rather than α (one can of course always go easily from one to the other if needed using Eq. (57)).

Deflagrations/hybrids To explore the properties of deflagration and hybrid solutions we perform a scan varying α_p and b while keeping m_{\pm} fixed. The result of this scan is shown in Fig. 3, with $m_+ = 0$ and $m_- = T_n$ on the left panels and $m_+ = 0$ and $m_- = \infty$ (more formally $m_- \gg \gamma_w T_n$) on the right panels. The former is meant to represent a typical electroweak PT (with the Higgs acquiring a VEV $v \sim T_n$), while the latter corresponds to the large mass limit

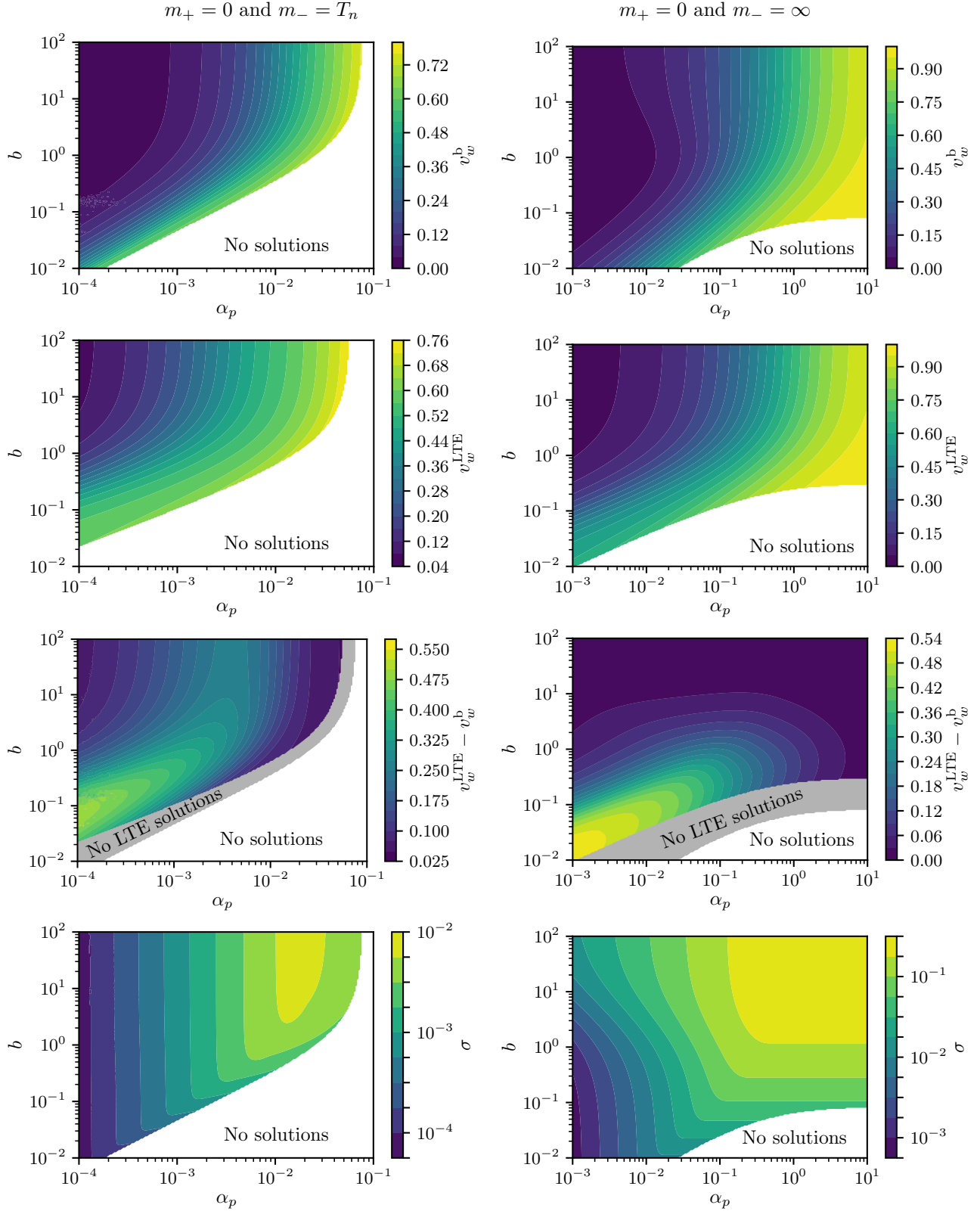


Figure 3: Contour plots of scans varying the parameters α_p and b with fixed m_+ and m_- for deflagration and hybrid solutions only. They show (from top to bottom) the ballistic solution v_w^b , the LTE solution v_w^{LTE} , the difference between the ballistic and LTE solutions $v_w^{LTE} - v_w^b$ and the entropy fraction generated by the ballistic solution σ . The left side is with $m_+ = 0$ and $m_- = T_n$, and the right side with $m_+ = 0$ and $m_- = \infty$ (the large mass limit).

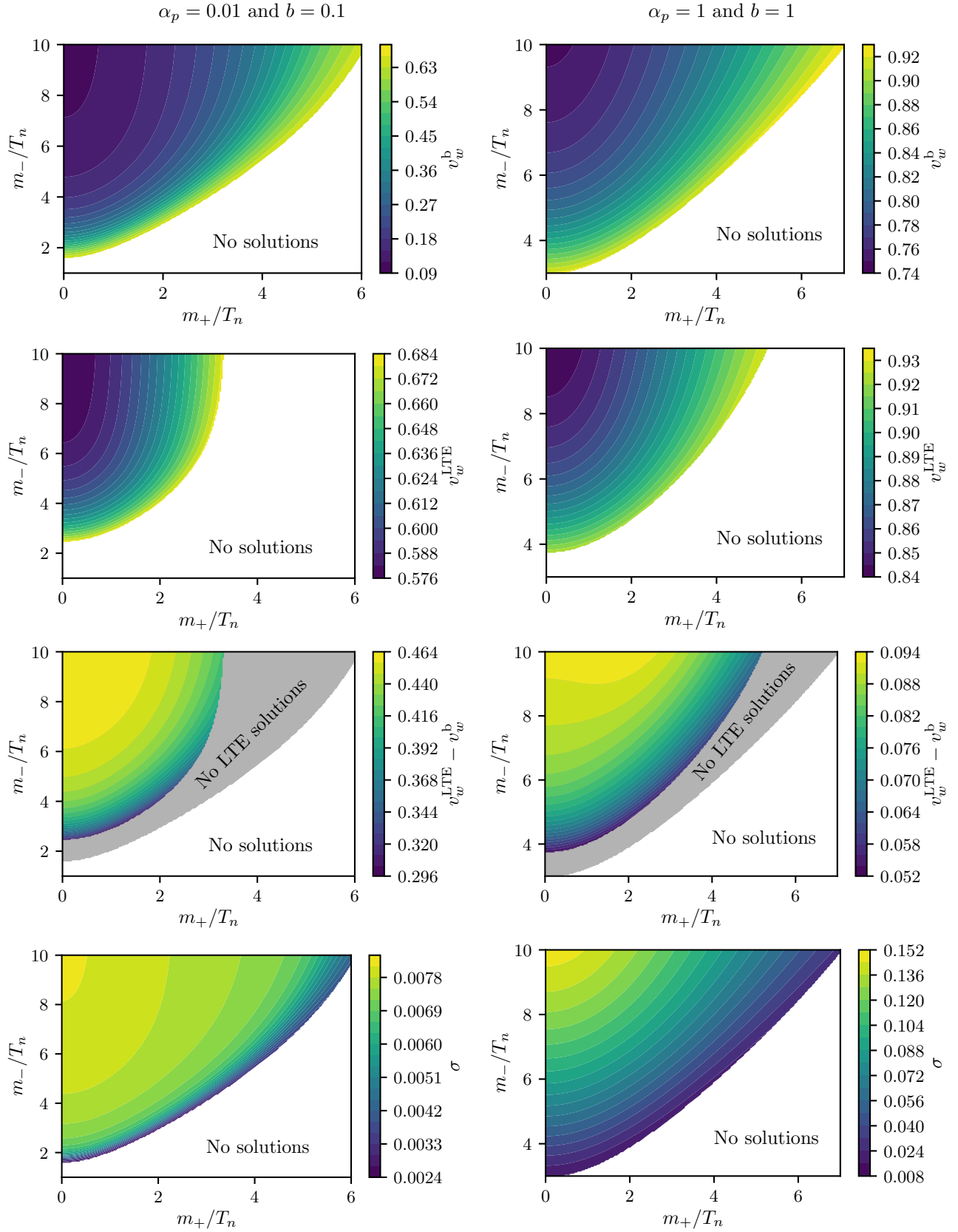


Figure 4: Contour plots of scans varying the parameters m_+ and m_- with fixed α_p and b for deflagration and hybrid solutions only. They show the same quantities as in Fig. 3. The left side is for a rather weak PT with $\alpha_p = 0.01$ and $b = 0.1$, while the right side is for a stronger PT with $\alpha_p = 1$ and $b = 1$.

(LML) which has interesting properties that will be discussed in the next subsection. For these two cases, one has $\Psi(T_n) \approx (1 + 0.89b)/(1 + b)$, $\Psi(T_n) = 1/(1 + b)$, respectively. This means that the parameter b has a very different implication in these two cases. For the former Ψ can never be smaller than 0.89, while for the latter, it can be as small as 0.

The first two rows of Fig. 3 show the wall velocity computed in the ballistic limit v_w^b and in LTE v_w^{LTE} . In all cases, we can see white regions where no deflagration or hybrid solutions were found. In these regions, the PTs are simply too strong and the plasma too weakly coupled to create substantial friction on the wall. The wall is therefore free to accelerate beyond the Jouguet velocity and become a detonation or possibly a runaway solution. The part of parameter space where a solution can be found is always larger when the ballistic approximation is used rather than LTE, since the friction in the first case is higher and can therefore stop the wall more easily. Note that the same conclusion does not hold if one uses the Bödeker-Moore 1-to-1 thermal friction (30). This means that the asymptotic value of the pressure in the $\gamma_w \rightarrow \infty$ (when only the 1-to-1 processes are considered) is not necessarily larger than the pressure peak at the Jouguet velocity [114].

Note that the $m_- = T_n$ and $m_- = \infty$ cases behave in a very different way. In the former, there is a maximal value of α_p beyond which no deflagration or hybrid solutions are possible. In the second case, if b is high enough, there will always be such a solution no matter how strong the PT is. This fact was first observed in Ref. [80] for LTE, and we can observe here that it can also happen in the ballistic limit. Note however that the ballistic wall velocity can only be interpreted as an upper bound as long as the size of the shock wave is larger than L_{MFP} .

The third row of Fig. 3 shows the difference between v_w^{LTE} and v_w^b . An important observation is that, in most of the parameter space, both limits agree on the type of solution. Effectively, they both agree that a deflagration/hybrid solution exists in the colored region and that no solution exists in the white region (which means the wall must be a detonation or runaway). They only disagree in the narrow grey band where a ballistic solution can be found but no LTE one. This implies that, away from this grey band, it is possible to determine with certainty the solution type of a general model: deflagration/hybrid if a solution exists in LTE, and detonation if no solution exists in ballistic.

If there is a solution in LTE, then the true wall velocity v_w is in the interval $[v_w^b, v_w^{\text{LTE}}]$. A simple estimate of v_w can then be obtained with, e.g., $v_w^{\text{mean}} = (v_w^b + v_w^{\text{LTE}})/2$. As can be seen in Fig. 3, the difference between v_w^b and v_w^{LTE} can be quite large in some parts of the parameter space, and v_w^{mean} could be off by at most ~ 0.3 . If that is the case, solving the Boltzmann equations could be necessary if more precision is needed. There are two regimes where v_w^b and v_w^{LTE} are approximately equal. The first one happens when $\Psi \approx 0$ (or $b \gg 1$ and $m_- - m_+ \gg T_n$) where, as argued in Section 4.1, $\Psi_{\text{eff}} \approx \Psi$ and the entropy production has no effect on the wall velocity. v_w^{mean} also becomes exact when $\alpha_n \gg 1/3$ simply because both v_w^b and v_w^{LTE} approach 1 for strong PTs. Both of these two cases can be seen on the right side of Fig. 3. If a model is in one of these two situations (which often happens in confining PTs or in models with conformal invariance), solving the Boltzmann equations may become unnecessary as v_w^b and v_w^{LTE} agree very well.

Finally, the fourth row of Fig. 3 shows the entropy production fraction σ (Eq. (34)) obtained

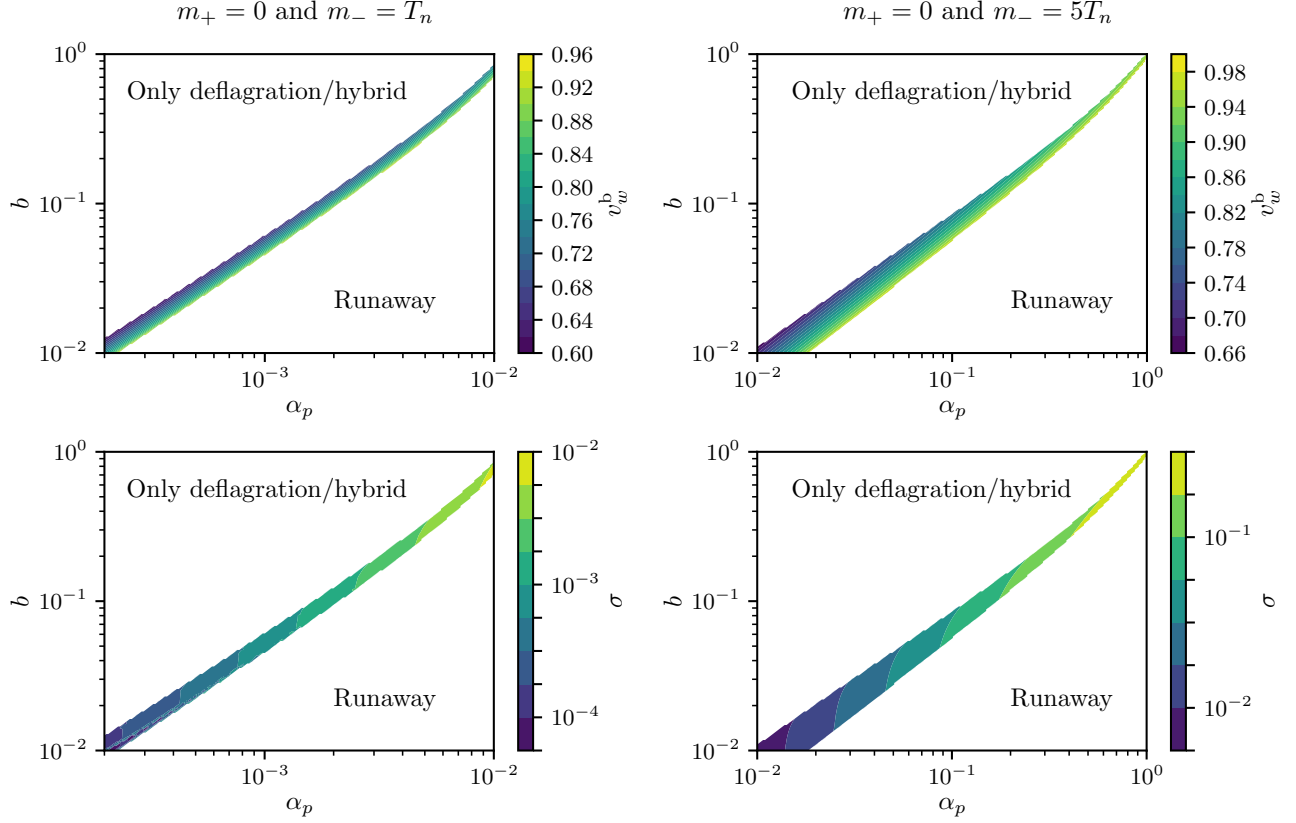


Figure 5: Contour plots of scans varying the parameters α_p and b with fixed m_+ and m_- for detonation solutions only. They show the ballistic solution v_w^b and the entropy fraction generated σ . The left side is with $m_+ = 0$ and $m_- = T_n$, and the right side with $m_+ = 0$ and $m_- = 5T_n$.

in the ballistic approximation. This quantity can be useful to quantify the extent to which the plasma can be out-of-equilibrium. It can also be used to compute Ψ_{eff} which allows one to describe mathematically the model using the LTE formalism, even if the plasma has deviations from equilibrium. Furthermore, σ always vanishes in LTE, while it is maximized in the ballistic limit, so the true entropy produced must always be smaller than the value shown here.

We show different scans in Fig. 4 where α_p and b are held fixed and m_{\pm} are varied. Again, there are two different scans: one with $\alpha_p = 0.01$ and $b = 0.1$ which are typical values obtained in the singlet scalar extension of the SM, and the other one with $\alpha_p = 1$ and $b = 1$ which represents a stronger PT. One can observe that the wall velocity is minimized in the LML (the upper left corner), where the mass variation is maximal. This is not surprising as the large mass variation creates a large friction that slows down the wall more efficiently. Furthermore, it can be seen that having a deflagration or hybrid solution requires having a relatively small value of m_+ . If it is too large, the particles are completely Boltzmann suppressed in front of the wall and they cannot generate any pressure, even if $m_- \gg m_+$. We note, however, that both $v_w^{\text{LTE}} - v_w^b$ and σ are maximized in the LML.

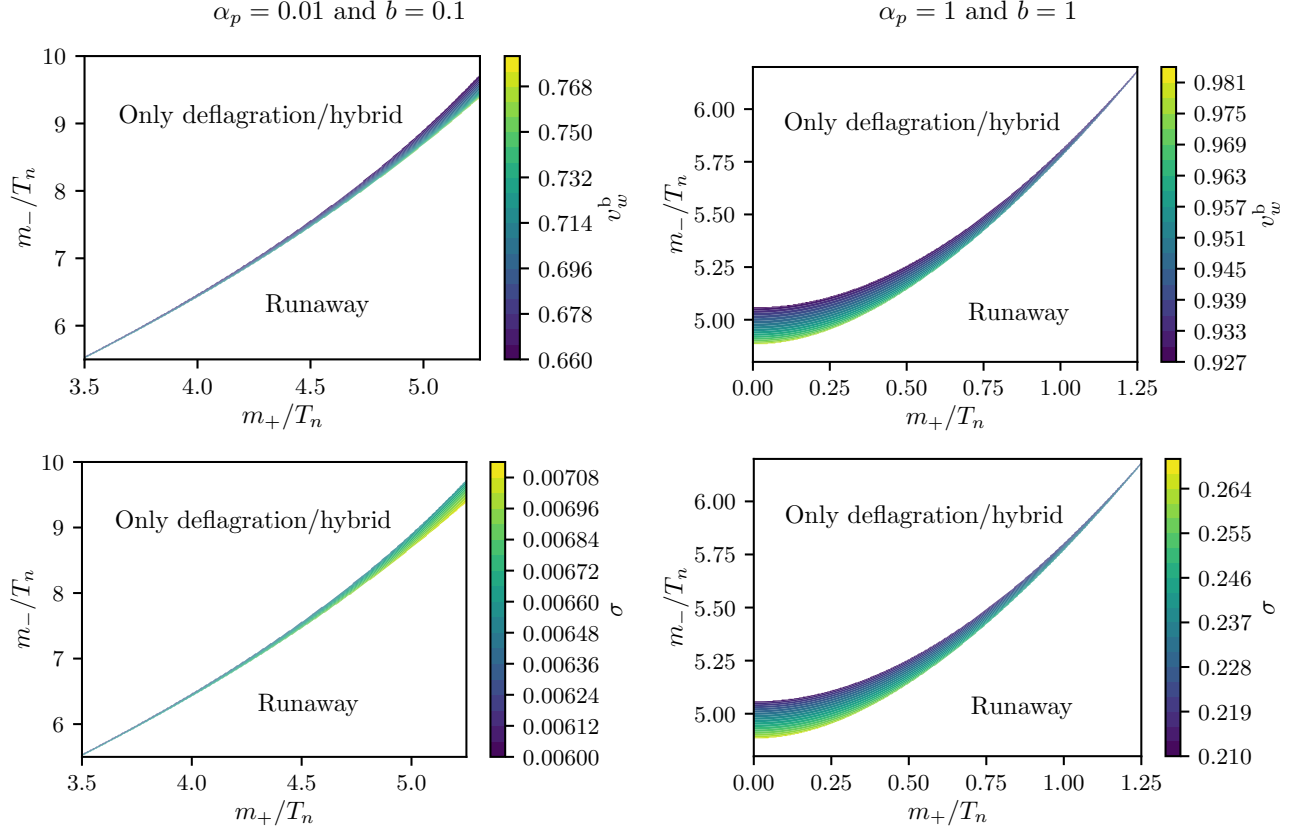


Figure 6: Same as in Fig. 5 but varying m_{\pm} with $\alpha_p = 0.01$ and $b = 0.1$ (left) and $\alpha_p = b = 1$ (right).

Detonations We now move to describe the detonation solutions. In contrast to deflagration and hybrid solutions, it was shown in Ref. [80] that stable detonations do not occur in LTE. This is because in LTE the net pressure $\mathcal{P}_{\text{friction}}(v_w) - \mathcal{P}_{\text{driving}}$, is a monotonically decreasing function of v_w after the Jouguet velocity. Even though there is a solution $\mathcal{P}_{\text{friction}}(v_w) - \mathcal{P}_{\text{driving}} = 0$ for $v_w > v_J$, it cannot be stable. On the other hand, we will see shortly that detonations do occur in the ballistic limit as now the net pressure is not monotonically decreasing above v_J (see Fig. 8 below for an example). There are even parameter points with several detonation solutions, but for simplicity, we will only consider the solution with the smallest wall velocity in what follows.

We show in Figs. 5 and 6 the same scans as for the deflagration and hybrid branch. It is quite clear from these scans that finding a stable static detonation solution requires some amount of fine-tuning. If the PT is too weak, the driving force on the wall will simply be too small to overcome the friction in the detonation regime. In that case, the net pressure on the wall is always positive for $v_w \in [v_J, 1)$ and the only possible solutions are deflagrations or hybrids. On the other hand, in the detonation regime the friction generated by the plasma cannot be arbitrarily large (see the Bödeker-Moore limit in Sec. 3.2), so if the PT is too strong, the net pressure will always be negative for $v_w > v_J$. In that case, although no static detonations can be found, the wall can become a runaway as the negative pressure will continue pushing the wall forward until it reaches an ultrarelativistic speed.

5.1.2 Large mass limit

An interesting case happens when the massive particles start nearly massless in the symmetric phase and end up very heavy in the broken phase, which corresponds to the limit $m_+ \rightarrow 0$ and $m_- \rightarrow \infty$ (or more specifically, $m_- \gg \gamma_+ T_+$). This type of situation can naturally occur in models where a scalar field acquires a very large VEV (e.g. in conformal models) or in confining PTs.⁹ In this large mass limit (LML), the plasma only contains massless particles everywhere, as the heavy particles are completely Boltzmann suppressed in the broken phase, which thus only contains the massless species. As we will see, this fact drastically simplifies the analysis.

The LML is not only simpler to analyze, it also provides an interesting limit. For a fixed value of α_p (or α_n) and b , it becomes clear from the second row of Fig. 4 that the LML gives the smallest value of the wall velocity. The LML thus provides us with a lower bound on the ballistic wall velocity, which was already the lower bound on the wall velocity. Put in another way, the LML gives the lowest lower bound on the wall velocity among all particle physics models with a fixed α_p and b .

Let us now demonstrate how the analysis simplifies in the LML. A first simplification occurs for the equation of state of the LML. Since the plasma is completely radiation-dominated, we always have $c_s^2/b = 1/3$. This implies that the plasma can be represented perfectly by the bag EoS. As mentioned before, $\Psi = 1/(1+b)$ for this case. Notice that these thermodynamic quantities are all temperature-independent, which is not generally the case.

The second simplification happens in the calculation of the ballistic pressure. Because $m_- \rightarrow \infty$, it can be seen in Eqs. (28) that only the contribution from reflections \mathcal{P}^r is nonvanishing. Furthermore, the integral can be performed analytically which gives a total friction force on the wall,

$$\mathcal{P}_{\text{friction}}(T_+, v_+) = \frac{\pi^2 g_{\star, \phi} T_+^4}{90} (1 + v_+)^3 \gamma_+^2 = \frac{1 - \Psi}{4} \omega_+(T_+) (1 + v_+)^3 \gamma_+^2. \quad (58)$$

Notice that this pressure asymptotically grows like γ_+^2 when $v_+ \rightarrow 1$, and can therefore be arbitrarily large. Therefore, there are no runaway solutions in the LML. This seems to be in contradiction with the Bödeker-Moore limit [106] mentioned in Section 3.2, which predicts a finite pressure in the $v_+ \rightarrow 1$ limit. This discrepancy is a consequence of the order in which the two limits are taken. By taking the LML first, we implicitly assume $m_-/T_+ \gg \gamma_+$, which gives the friction (58). On the other hand, Bödeker-Moore assumes $m_-/T_+ \ll \gamma_+$, which gives Eq. (30). In realistic models, m_- can be large, but it is finite. Thus, the LML cannot be valid up to $v_+ = 1$ and for a large enough wall velocity, the Bödeker-Moore limit will become the correct description. We will however not consider such complications and focus on the pure LML in what follows.

⁹At first glance, the ballistic treatment seems not particularly useful in the confining case. Particles cannot simply be tracked from the deconfined phase into the confining phase, since both phases contain completely different degrees of freedom. In the limit $m_- \rightarrow \infty$ however, only particles in the deconfined phase are relevant, and the ballistic approximation can be used to describe those.

By requiring that $\mathcal{P}_{\text{driving}} = \mathcal{P}_{\text{friction}}$, one can derive a new condition valid in the ballistic LML:

$$\alpha(T_+) = \frac{1 - \Psi}{3}(1 + v_+)^3 \gamma_+^2. \quad (59)$$

Interestingly, this condition only depends on the plasma velocity and temperature measured in front of the wall.

Detonations For detonation solutions which have $v_+ = v_w$ and $T_+ = T_n$, the wall velocity can be determined directly to be

$$v_w^{\text{det}} = \frac{\sqrt{3\alpha_n[8(1 - \Psi) + 3\alpha_n]} - 3\alpha_n}{2(1 - \Psi)} - 1. \quad (60)$$

For this solution to be valid, it must be larger than the Jouguet velocity [80]

$$v_J = \frac{1}{\sqrt{3}} \left(\frac{1 + \sqrt{\alpha_n(2 + 3\alpha_n)}}{1 + \alpha_n} \right), \quad (61)$$

otherwise, a shock wave would form in front of the wall and the solution would be a deflagration or hybrid wall, not a detonation. This implies that to have a detonation solution in the LML, one must satisfy

$$\Psi_{\text{det}} > 1 - \frac{3\alpha_n(1 - v_J)}{(1 + v_J)^2}. \quad (62)$$

In particular, one can show that this bound is minimal when $\alpha_n \rightarrow \infty$, in which case the bound becomes $\Psi_{\text{det}} > (2 + \sqrt{3})/4 \approx 0.933$. Therefore, in the ballistic LML, no detonation solution can exist if Ψ is smaller than 0.933 no matter what α_n is. For $\Psi < 0.933$, the wall velocity would be too slow to prevent a shock wave from forming, and the solution would eventually become a hybrid or deflagration.

As mentioned earlier, in realistic situations m_- cannot be infinite. Therefore, the above conclusion is valid only for

$$\frac{m_-}{T_n} \gg \gamma_w^{\text{det}}, \quad (63)$$

which gives an additional condition for m_-/T_n for given α_n and Ψ . In Fig. 7, we show γ_w^{det} together with the condition (62). It can be seen that for the plotted $\alpha_p \lesssim 100$, a value of m_-/T_n of order $\mathcal{O}(10) - \mathcal{O}(100)$ would justify the conclusion that there is no detonation solution when $\Psi \lesssim 0.933$.

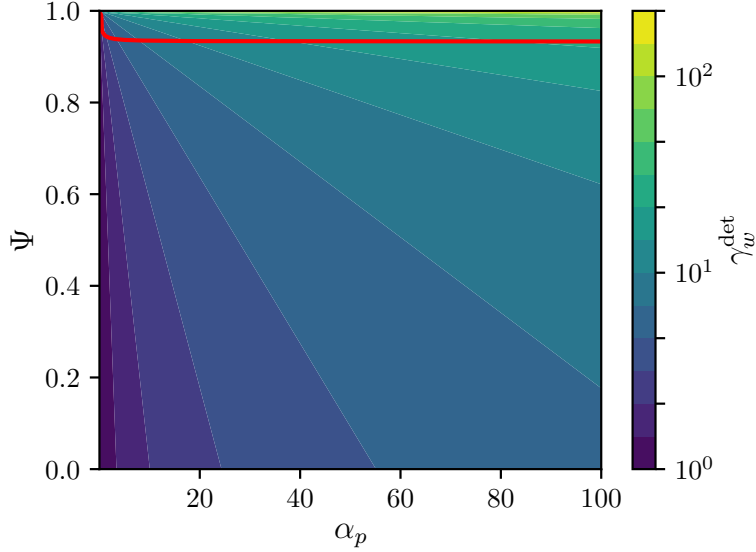


Figure 7: Contour plot of $\gamma_w^{\text{det}}(\alpha_p, \Psi)$ for the velocity given in Eq. (60). The region below the red line violates the condition (62). If further m_-/T_n is much larger than γ_w^{det} , then there is no detonation solution for the parameter region below the red line.

Deflagrations/hybrids The situation for deflagration and hybrid solutions is more complicated since they have a shock wave propagating in front of the wall, so one cannot directly relate v_+ and T_+ to v_w and T_n . Nevertheless, one can use the new condition (59) to compute the entropy production fraction σ defined in Eq. (34). As described in Section 4.1, this will allow us to treat the system like it is in LTE, but with an effective value of Ψ

$$\Psi_{\text{eff}} = \frac{\Psi}{(1 + \sigma)^4}. \quad (64)$$

This thus gives us a direct way to compare LTE to ballistic, since they can be treated mathematically identically.

First, one can eliminate T_- from the definition of σ by substituting Eq. (10a) into (34) and (32). By assuming that the plasma is described by the bag EoS (which is always the case in the LML), one can show that

$$\sigma = \left(\frac{\gamma_+^2 v_-}{\gamma_-^2 v_+} \Psi \right)^{1/4} - 1. \quad (65)$$

One can then substitute Eq. (59) into (A77b) to obtain a matching equation independent of T_- and T_+ . It can be expressed in terms of the cubic equation

$$0 = (1 - \Psi)v_-v_+^3 - 3\Psi v_-v_+^2 + [1 + 3v_-(1 + v_- - \Psi)]v_+ - \Psi v_-. \quad (66)$$

In principle, one could use Cardano's formula to solve this cubic equation for v_+ and substitute the result into Eq. (65) to express σ completely in terms of Ψ and v_w (remember that $v_- = v_w$

for deflagrations and $v_- = c_b = 1/\sqrt{3}$ for hybrids). However, the resulting expression is quite complicated which makes it challenging to analyse and understand its qualitative behavior.

What will be much more instructive is to study different limiting cases. In particular, we will be interested in the small v_- , small Ψ and small $1 - \Psi$ limits. In these limits, the solution of Eq. (66) is

$$v_+ = \begin{cases} \frac{v_- \Psi}{1 + 3v_-(1 + v_- - \Psi)}, & v_- \ll 1 \text{ or } \Psi \ll 1, \\ v_- - \frac{v_-(1 + v_-)^3(1 - \Psi)}{1 - 3v_-^2}, & 1 - \Psi \ll \frac{1}{\sqrt{3}} - v_-. \end{cases} \quad (67)$$

Substituting these into Eq. (65), one obtains the entropy production fraction

$$\sigma = \begin{cases} \frac{(3 + v_-)}{4(1 - v_-)} v_- (1 - \Psi), & v_- \ll 1 \text{ or } 1 - \Psi \ll 1, \\ \frac{f(v_-)}{\sqrt{\gamma_-}} - 1 - \frac{3v_- \Psi}{4f^3(v_-)\sqrt{\gamma_-}}, & \Psi \ll 1, \end{cases} \quad (68)$$

with $f(v_-) = [1 + 3v_-(1 + v_-)]^{1/4} \approx 1 + 0.675v_-$.

There are a few interesting consequences of these limiting behaviours. First, σ always vanishes when $v_- = 0$ or $\Psi = 1$. Also, it is an increasing function of v_- and a decreasing function of Ψ . This implies that for deflagration and hybrid solutions, σ is maximized when $\Psi = 0$ and $v_- = 1/\sqrt{3}$, at which point it takes the value $\sigma_{\max} = f(1/\sqrt{3})(2/3)^{1/4} - 1 \approx 0.256$. Because the pressure in the ballistic LML is the absolute maximum a PT with a fixed α_p and b can have, σ_{\max} is actually the largest entropy fraction a PT with deflagration or hybrid expansion can produce, no matter what the model is and whether it is best described by LTE, ballistic, or anything in between. However, note that for detonations, it can be shown that σ grows asymptotically like $\alpha^{1/4}$ and can therefore be arbitrarily large.

Starting from Eq. (68), it is quite easy to find a numerical fit that approximates σ well for every value of Ψ and v_- . For example, a good fit can be obtained with the simple function

$$\sigma_{\text{fit}} = \left(\frac{f(v_-)}{\sqrt{\gamma_-}} - 1 \right) \frac{1 - \Psi}{1 - Av_- \Psi}, \quad (69)$$

with $A \approx 0.91$ giving the best fit with a maximal error of less than 1% for $\Psi \in [0, 1]$ and $v_- \in [0, 1/\sqrt{3}]$. Furthermore, this fit is exact when $\Psi = 0, 1$ or $v_- = 0$. Once we have σ_{fit} , we can substitute it into Eq. (64) to get $\Psi_{\text{eff}}(T_n)$ for a given $\Psi(T_n)$. Then substituting $\Psi_{\text{eff}}(T_n)$ into the fit formula for the LTE wall velocity given in Ref. [80], we obtain the resulting wall velocity. Note that we are only using the correspondence mentioned in Sec. 4.1 and are still deriving the ballistic wall velocity here.

5.2 Example model: the Standard Model coupled to a gauge singlet

Let us now put our approximations to the test in a concrete example model. We choose the \mathbb{Z}_2 -symmetric xSM, where the Standard Model Higgs h is coupled to a new gauge singlet s (see e.g. Refs. [7, 75, 117–119]), with tree level potential

$$V(h, s) = -\frac{\mu_h^2}{2} h^2 + \frac{\lambda_h}{4} h^4 + \frac{1}{2} \left(m_s^2 - \frac{\lambda_{hs} v^2}{2} \right) s^2 + \frac{\lambda_s}{4} s^4 + \frac{\lambda_{hs}}{4} h^2 s^2, \quad (70)$$

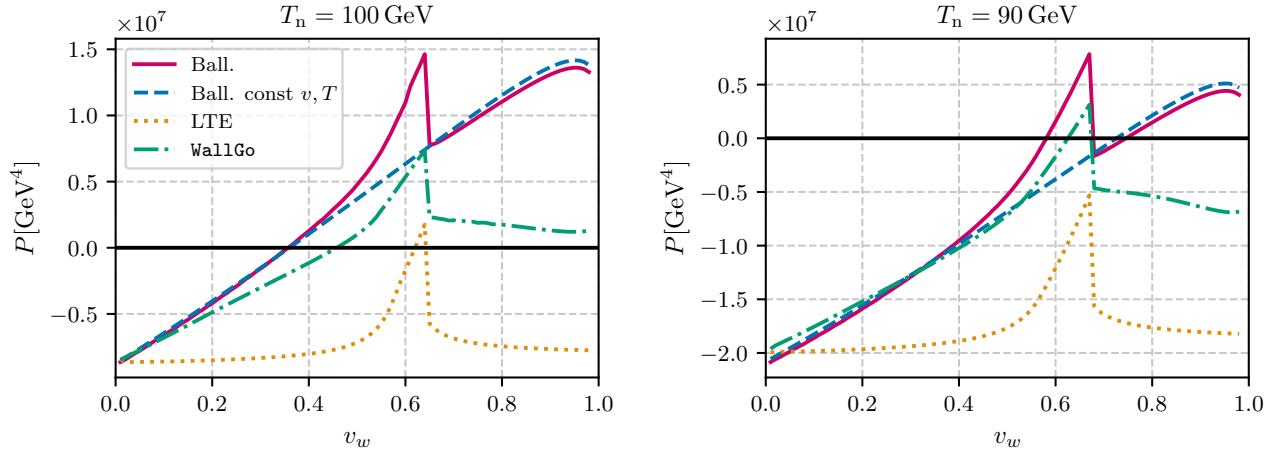


Figure 8: Pressure as a function of the wall velocity in four different approximations for the xSM.

where $v = \mu_h/\sqrt{\lambda_h} = 246$ GeV is the VEV of the SM Higgs h . m_s is the mass of the scalar singlet s at the vacuum $(v, 0)$ given by $\langle h \rangle = v, \langle s \rangle = 0$. We consider a region of parameter space where the PT proceeds in two steps: first, the singlet obtains a VEV, and in the second step, the Higgs obtains a VEV and the singlet goes back to zero. We use Benchmark 1 defined in Ref. [91], with $m_s = 120$ GeV, λ_{hs} and $\lambda_s = 1$ and focus on the second step of the PT for two choices of the nucleation temperature $T_n = 90, 100$ GeV.

We implement the one-loop effective potential as in Ref. [91]¹⁰ (based on Refs. [66, 75]): we include the one-loop thermal functions without high-temperature expansion, and the Coleman-Weinberg potential, with a RG-scale at 125.0 GeV. We include contributions to the one-loop effective potential from the singlet, Higgs, Goldstones, W - and Z -bosons and the top quark. We take the absolute value of the masses to avoid imaginary contributions to the effective potential. We do not consider running couplings or daisy resummation. Note that this treatment of the effective potential is expected to give rather large uncertainties [120–122], but also note that a computation of the wall velocity with a consistent inclusion of higher-order corrections to the effective potential has not yet been performed, and we therefore stick here with the one-loop effective potential.

In Fig. 8, we compare the pressure obtained in four different approaches for $T_n = 100$ GeV (left) and $T_n = 90$ GeV (right):

1. The ballistic approximation, as discussed in this work (solid magenta). We include the contributions from the singlet, Higgs, Goldstone, W - and Z -bosons and the top quark. The singlet loses mass when it enters the bubble, and we therefore use the expressions of Appendix C to include its contribution to the pressure.
2. The ballistic approximation with the same contributing particles, under the approximation that $v_+ = v_- = v_w$ and $T_+ = T_- = T_n$ (dashed blue).

¹⁰The relevant model file can be found in the `Models/SingletStandardModel_Z2` .

3. Solution to the scalar field EoM in LTE (dotted yellow).
4. Solution of the scalar field EoM, with friction from the top quark, without assuming the ballistic approximation (dash-dotted green).

To obtain pressures 1, 3 and 4, we make use of the code `WallGo` [91]. For the ballistic approximation, we only extract the hydrodynamic matching relations (T_+, T_-, v_+, v_-) as a function of v_w and compute the pressure using Eqs. (26). For 3 and 4, the pressure is directly returned by `WallGo`. In the computation, the bubble profile is approximated by a Tanh-ansatz, and the pressure for each wall velocity is determined by finding the wall widths and offsets that minimize the action (see Ref. [68] for further details on this approach). Note that there is a slight ambiguity in the definition of the pressure, because the static equation of motion can not be applied for arbitrary v_w . This ambiguity might explain why the different approximations do not go to exactly the same value of P at $v_w \rightarrow 0$. Another possible reason for the small difference at $v_w \rightarrow 0$ is that `WallGo` has been configured to return the principal part of the potential for a negative mass squared, whereas we take the absolute value in the ballistic computation.

For $T_n = 100$ GeV, the four different approximations for the pressure yield $v_w = 0.36, 0.36, 0.62, 0.46$, for ballistic, ballistic with constant v and T , LTE and `WallGo` respectively. For $T_n = 90$ GeV, we have $v_w = 0.58$ (ballistic), 0.73 (ballistic, constant v and T), 0.63 (`WallGo`), while in LTE no static solution is found.

As anticipated, the pressure is smallest, and the wall velocity largest in the LTE approximation for both choices of nucleation temperature. We also see that the ballistic approximation with v_w -dependent temperature and fluid velocity gives the largest estimate of the pressure. The pressure with out-of-equilibrium top quark, with the (leading log) collision integrals falls in between the two approximations. Interestingly, the ballistic approximation of Refs. [65, 94] (with fixed temperature and wall velocity) reproduces v_w of our updated ballistic approximation very well for $T_n = 100$ GeV, but it underestimates the pressure for $T_n = 90$ GeV. As a result, it overestimates the wall velocity, and finds a detonation solution rather than a hybrid.

6 Conclusions

The LTE and ballistic approximations are two approaches for estimating bubble wall velocities in FOPTs. These approximations are typically applicable within specific regions of the parameter space and wall velocities. For instance, the LTE approximation is generally reliable for relatively low wall velocities ($\gamma_w \lesssim \mathcal{O}(10)$) and strong interactions among plasma particles. In contrast, the ballistic approximation is suitable in scenarios with either very weak interactions or very high wall velocities (i.e., when $\gamma_w \gg 1$). In this work, however, we use these approximations to derive general bounds on friction and wall velocity. The two limits correspond to extreme collision rates: $\Gamma \rightarrow 0$ for the ballistic regime and $\Gamma \rightarrow \infty$ for LTE. By linearising the general Boltzmann equation, we have analytically demonstrated that the LTE and ballistic limits indeed establish upper and lower bounds on the wall velocity, respectively, so that $v_w \in [v_w^b, v_w^{\text{LTE}}]$.

As a key development in this work, we have demonstrated how hydrodynamics effects can be incorporated into the ballistic approximation. To achieve this, we account for inhomogeneities

in the fluid temperature and velocity while solving the Liouville equation, i.e., the collisionless Boltzmann equation. The resulting general solution depends on $\{T_{\pm}, v_{\pm}\}$, where T_{\pm} and v_{\pm} denote the fluid temperature and velocity in front of/behind the bubble wall, respectively. From this solution for the particle distribution functions, we compute the friction on the wall, $\mathcal{P}_{\text{friction}}^{\text{b}}(T_+, T_-, v_+, v_-)$. We have further shown that $\mathcal{P}_{\text{friction}}^{\text{b}} = \mathcal{P}_{\text{driving}} \equiv \Delta V$ can serve as an additional matching condition, enabling us to fully determine the wall velocity. With hydrodynamics correctly integrated, we demonstrate that the ballistic pressure exhibits a non-monotonic behavior, featuring a local peak at the Jouguet velocity. This finding aligns with previous observations made using the LTE approximation or the complete solution of the Boltzmann equation [68, 74, 75, 113, 114].

We have conducted an extensive scan for the wall velocities obtained in the two approximations in a model-independent framework. We identify parameter regions with a small difference in the two solutions ($v_w^{\text{LTE}} - v_w^{\text{b}}$), where solving the full Boltzmann equation is not necessary, and those with a relatively large difference. For deflagration/hybrid motions, we have observed that in some part of parameter space, there are ballistic solutions but no LTE ones. This is reasonable as the ballistic pressure is always larger than the LTE pressure so there are situations in which the ballistic pressure can beat the driving pressure before reaching the Jouguet velocity while the LTE pressure cannot. While it has been shown in the previous work [80] that there is no stable detonation solution in LTE, we have shown that this is not the case for the ballistic approximation, although the parameter space allowing for such solutions is relatively narrow. For the ballistic approximation, we also provide a detailed analysis of cases where particles become very massive after entering the bubble, as occurs in models with conformal symmetry, for example. In these instances, we offer either an analytic solution for the wall velocity in the detonation case or a numerical fit for deflagration and hybrid cases. Finally, we have applied our methods to a specific model: the Standard Model coupled to a gauge singlet, and obtained the wall velocities in different limits, comparing them with the one obtained from solving the full Boltzmann equation using the package `WallGo` recently released in Ref. [91]. For the benchmark point we considered, we have seen that the velocity obtained by solving the full Boltzmann equation does lie between the LTE and ballistic bounds.

Our analysis remains valid as long as hydrodynamics applies. However, we have taken Eq. (1a) as our starting point, which accounts for the friction arising from condensate-dependent mass terms only. There may also be condensate-dependent vertices, such as $\phi\eta\chi^2$ (where η represents the fluctuation field of the order-parameter scalar upon the bubble background), that could induce particle production processes like $\eta \rightarrow \chi\chi$. These processes and the resulting friction can be captured by self-energy modifications to Eq. (1a). We anticipate that these additional contributions remain subdominant at relatively low values of γ_w . For cases with $\gamma_w \rightarrow \infty$, however, these modifications would need to be taken into account. For a detailed analysis of bubble wall dynamics including self-energy corrections in the scalar EoM, see Refs. [123, 124].

Acknowledgments

WYA is supported by the UK Engineering and Physical Sciences Research Council (EPSRC), under Research Grant No. EP/V002821/1. BL is supported by the Fonds de recherche du Québec Nature et technologies (FRQNT). JvdV is supported by the Dutch Research Council (NWO), under project number VI.Veni.212.133.

A Model-independent hydrodynamics with the template EoS

To have a model-independent analysis, one usually introduces an EoS for the plasma. A good EoS is the so-called template model [115] that has been used in various studies [80, 85, 125]). As a generalization of the bag model, the template model allows the sound speeds in both phases to deviate from $1/\sqrt{3}$. Explicitly, it reads

$$e_s(T) = \frac{1}{3}a_+(\mu - 1)T^\mu + \epsilon, \quad p_s(T) = \frac{1}{3}a_+T^\mu - \epsilon, \quad (\text{A71})$$

$$e_b(T) = \frac{1}{3}a_-(\nu - 1)T^\nu, \quad p_b(T) = \frac{1}{3}a_-T^\nu, \quad (\text{A72})$$

where the constants μ, ν are related to the sound speed in the symmetric and broken phases through

$$\mu = 1 + \frac{1}{c_s^2}, \quad \nu = 1 + \frac{1}{c_b^2}. \quad (\text{A73})$$

For $\mu = \nu = 4$, it reduces to the bag EoS.

To formulate the matching conditions in terms of model-independent parameters, we introduce the D operator through [125]

$$\begin{aligned} \Delta p &= p_s(T_+) - p_b(T_-) = [p_s(T_+) - p_b(T_+)] + [p_b(T_+) - p_b(T_-)] \\ &\equiv Dp(T_+) + \delta p(T_+, T_-), \end{aligned} \quad (\text{A74})$$

and similarly for the energy density and enthalpy. Above we have defined $Dp(T) \equiv p_s(T) - p_b(T)$, the difference of a thermodynamic quantity in the two phases but at the same temperature. δp depends on T_+ and T_- but only involves quantities in the broken phase. A quantity that turns out to be of particular importance is

$$\frac{\delta p(T_+, T_-)}{\delta \rho(T_+, T_-)} = \frac{p_b(T_+) - p_b(T_-)}{e_b(T_+) - e_b(T_-)} \equiv \zeta^2(T_+, T_-). \quad (\text{A75})$$

In the template EoS, we have $\zeta(T_+, T_-) = c_b$ which is constant.

Ref. [125, 126] then introduces the following quantity for the PT strength

$$\alpha(T) = \frac{D\bar{\theta}}{3\omega_s(T)}, \quad \bar{\theta} = \left(e - \frac{p}{c_b^2} \right). \quad (\text{A76})$$

With the parameter $\alpha_+ \equiv \alpha(T_+)$, one can write the matching conditions as

$$\frac{\Delta p}{3\omega_+} \left(1 - \frac{v_+v_-}{\zeta^2} \right) = v_+v_- \alpha_+, \quad (\text{A77a})$$

$$\frac{v_+}{v_-} = \frac{\left(\frac{v_+v_-}{\zeta^2} - 1 \right) + 3\alpha_+}{\left(\frac{v_+v_-}{\zeta^2} - 1 \right) + 3v_+v_- \alpha_+}. \quad (\text{A77b})$$

We have now two constraint equations for five unknowns $\{v_w, v_+, v_-, T_+, T_-\}$. For detonations, T_+ and v_+ are equal to the nucleation temperature T_n and v_w , respectively. For deflagrations/hybrids, T_+ can be related to T_n through the fluid equations between the wall and the shock front, while there is an additional condition either through $v_- = v_w$, or $v_- = c_b$. One is essentially left with three unknowns. With the third constraint equation in the LTE or ballistic approximations (see Secs. 3.1 and 3.2), one then has a closed system of equations and all the unknowns can be determined, from which the wall velocity can be inferred.

For the LTE approximation, substituting Eq. (13) into (A77a) and using the EoS, one gets [80]

$$3\nu\alpha_+v_+v_- = \left[1 - 3\alpha_+ - \left(\frac{\gamma_+}{\gamma_-}\right)^\nu \Psi_+\right] \left(1 - \frac{v_+v_-}{c_b^2}\right), \quad (\text{A78})$$

where

$$\Psi(T) = \omega_b(T)/\omega_s(T) \quad (\text{A79})$$

and $\Psi_+ = \Psi(T_+)$. Now, T_- has been eliminated in the two matching conditions (A77b) (with $\zeta = c_b$) and (A78). As T_+ is related to T_n , either directly or through the fluid equations and matching conditions at the shock front, the system of equations is closed and one can determine the wall velocity for a given T_n . More specifically, for detonations, $T_+ = T_n$ and therefore $\alpha_+ = \alpha_n \equiv \alpha(T_n)$, $\Psi_+ = \Psi_n \equiv \Psi(T_n)$. For deflagrations/hybrids, one can first express α_+ or Ψ_+ in terms of α_n or Ψ_n from the template EoS

$$\alpha_+ = \frac{\mu - \nu}{3\mu} + \frac{\omega_n}{\omega_+} \left(\alpha_n - \frac{\mu - \nu}{3\mu}\right), \quad (\text{A80a})$$

$$\Psi_+ = \Psi_n \left(\frac{\omega_+}{\omega_n}\right)^{\nu/\mu-1}, \quad (\text{A80b})$$

and then compute ω_n/ω_+ by integrating the fluid equations. In conclusion, within the LTE approximation and the template model, the dynamics can be fully determined by four thermodynamic quantities: α_n , Ψ_n , c_s and c_b .

B Ballistic pressures for Bose-Einstein and Fermi-Dirac distributions

Here we present the expressions of \mathcal{P}^t , \mathcal{P}^{t+} and \mathcal{P}^{t-} for Bose-Einstein and Fermi-Dirac distributions, analogous to those given in Eqs. (28). We obtain

$$\mathcal{P}^{t+} = \frac{T_+^4}{4\pi^2\gamma_+} \int_{x>\sqrt{\Delta m^2/T_+}} dx x \left(x - \sqrt{x^2 - \Delta m^2/T_+^2} \right) \times \left[\pm\gamma_+ \left(\sqrt{x^2 + m_+^2/T_+^2} - v_+x \right) \mp \log \left(e^{\gamma_+(\sqrt{x^2 + m_+^2/T_+^2} - v_+x)} \mp 1 \right) \right], \quad (\text{B81a})$$

$$\mathcal{P}^{t-} = \frac{T_-^4}{4\pi^2\gamma_-} \int_{x>0} dx x \left(\sqrt{x^2 + \Delta m^2/T_-^2} - x \right) \times \left[\pm\gamma_- \left(\sqrt{x^2 + m_-^2/T_-^2} + v_-x \right) \mp \log \left(e^{\gamma_-(\sqrt{x^2 + m_-^2/T_-^2} + v_-x)} \mp 1 \right) \right], \quad (\text{B81b})$$

$$\mathcal{P}^r = \frac{T_+^4}{2\pi^2\gamma_+} \int_{0<x<\sqrt{\Delta m^2/T_+}} dx x^2 \left[\pm\gamma_+ \left(\sqrt{x^2 + m_+^2/T_+^2} - v_+x \right) \mp \log \left(e^{\gamma_+(\sqrt{x^2 + m_+^2/T_+^2} - v_+x)} \mp 1 \right) \right], \quad (\text{B81c})$$

where the upper/lower signs correspond to Bose-Einstein/Fermi-Dirac distributions.

C Particles that lose mass when entering the bubble

In certain scenarios, some of the particles actually *lose* mass, when entering the bubble. An example of this is the xSM, where the singlet becomes heavier in the singlet phase than in the Higgs phase. For these particles, the distribution functions associated with transmission and reflection are given by

- (1) Transmission from the symmetric phase (t_+):

$$f^{t+}(p^z, z; \mathbf{p}_\perp) = \frac{1}{e^{\beta_+\gamma_+(E-v_+\sqrt{p^{z2}+m^2(z)-m_+^2})} - 1}, \quad \left(p^z < -\sqrt{m_+^2 - m^2(z)} \right); \quad (\text{C82})$$

- (2) Reflection (r):

$$f^r(p^z, z; \mathbf{p}_\perp) = \frac{1}{e^{\beta_-\gamma_-(E+v_-\sqrt{p^{z2}+m^2(z)-m_-^2})} - 1}, \quad \left(-\sqrt{m_+^2 - m^2(z)} < p^z < \sqrt{m_+^2 - m^2(z)} \right); \quad (\text{C83})$$

- (3) Transmission from inside the bubble (t_-):

$$f^{t-}(p^z, z; \mathbf{p}_\perp) = \frac{1}{e^{\beta_-\gamma_-(E+v_-\sqrt{p^{z2}+m^2(z)-m_-^2})} - 1}, \quad \left(p^z > \sqrt{m_+^2 - m^2(z)} \right). \quad (\text{C84})$$

We see that m_- got replaced by m_+ in the conditions for p^z and that reflection now happens from the *inside* of the bubble.

The distribution at $z \rightarrow \infty$ is

$$f(p^z, \infty; \mathbf{p}_\perp) = \begin{cases} \frac{1}{e^{\beta_+ \gamma_+ (E+v+p^z)} - 1}, & p^z < 0, & (t^+\text{-modes}) \\ \frac{1}{e^{\beta_- \gamma_- (E+v-\sqrt{p^{z2}+\Delta\bar{m}^2})} - 1}, & p^z > 0, & (t^-\text{-modes}) \end{cases}, \quad (\text{C85})$$

where $\Delta\bar{m}^2 \equiv m_+^2 - m_-^2 = -\Delta m^2$. At $z \rightarrow -\infty$, we have

$$f(p^z, -\infty; \mathbf{p}_\perp) = \begin{cases} \frac{1}{e^{\beta_+ \gamma_+ (E-v+\sqrt{p^{z2}-\Delta\bar{m}^2})} - 1}, & p^z < -\sqrt{\Delta\bar{m}^2}, & (t^+\text{-modes}) \\ \frac{1}{e^{\beta_- \gamma_- (E+v-|p^z|)} - 1}, & -\sqrt{\Delta\bar{m}^2} < p^z < \sqrt{\Delta\bar{m}^2}, & (r\text{-modes}) \\ \frac{1}{e^{\beta_- \gamma_- (E+v-p^z)} - 1}, & p^z > \sqrt{\Delta\bar{m}^2}, & (t^-\text{-modes}) \end{cases}. \quad (\text{C86})$$

The different contributions to the pressure are given by

$$\mathcal{P}^{t_+} = \int_{p^z < 0} \frac{d^3\mathbf{p}}{(2\pi)^3} \frac{(p^z)^2}{E_+} f^{t_+}(p^z, +\infty) - \int_{p^z < -\sqrt{\Delta\bar{m}^2}} \frac{d^3\mathbf{p}}{(2\pi)^3} \frac{(p^z)^2}{E_-} f^{t_+}(p^z, -\infty), \quad (\text{C87a})$$

$$\mathcal{P}^{t_-} = \int_{p^z > 0} \frac{d^3\mathbf{p}}{(2\pi)^3} \frac{(p^z)^2}{E_+} f^{t_-}(p^z, +\infty) - \int_{p^z > \sqrt{\Delta\bar{m}^2}} \frac{d^3\mathbf{p}}{(2\pi)^3} \frac{(p^z)^2}{E_-} f^{t_-}(p^z, -\infty), \quad (\text{C87b})$$

$$\mathcal{P}^r = - \int_{|p^z| < \sqrt{\Delta\bar{m}^2}} \frac{d^3\mathbf{p}}{(2\pi)^3} \frac{(p^z)^2}{E_+} f^r(p^z, -\infty). \quad (\text{C87c})$$

These equations can be simplified by observing that $f^{t_\pm}(p^z, \pm\infty) = f^{\text{eq}}(p^z, \pm\infty)$, as before, and $f^{t_\pm}(p^z, \mp\infty) = f^{\text{eq}}(\mp\sqrt{p^{z2} \mp \Delta\bar{m}^2}, \pm\infty)$ and $f^r(p^z, -\infty) = f^{\text{eq}}(+|p^z|, -\infty)$

$$\mathcal{P}^{t_+} = \int_{p^z < 0} \frac{d^3\mathbf{p}}{(2\pi)^3} \frac{p^z}{E_+} \left(p^z + \sqrt{(p^z)^2 + \Delta\bar{m}^2} \right) f^{\text{eq}}(p^z, +\infty), \quad (\text{C88a})$$

$$\mathcal{P}^{t_-} = \int_{p^z > \sqrt{\Delta\bar{m}^2}} \frac{d^3\mathbf{p}}{(2\pi)^3} \frac{p^z}{E_-} \left(\sqrt{(p^z)^2 - \Delta\bar{m}^2} - p^z \right) f^{\text{eq}}(p^z, -\infty), \quad (\text{C88b})$$

$$\mathcal{P}^r = -2 \int_{0 < p^z < \sqrt{\Delta\bar{m}^2}} \frac{d^3\mathbf{p}}{(2\pi)^3} \frac{(p^z)^2}{E_+} f^{\text{eq}}(p^z, -\infty). \quad (\text{C88c})$$

Note that all the above pressures are now negative.

References

- [1] J. M. Cline and P.-A. Lemieux, “Electroweak phase transition in two Higgs doublet models,” *Phys. Rev. D* **55** (1997) 3873–3881, [arXiv:hep-ph/9609240](#).
- [2] M. Carena, M. Quiros, and C. E. M. Wagner, “Electroweak baryogenesis and Higgs and stop searches at LEP and the Tevatron,” *Nucl. Phys. B* **524** (1998) 3–22, [arXiv:hep-ph/9710401](#).
- [3] C. Grojean, G. Servant, and J. D. Wells, “First-order electroweak phase transition in the standard model with a low cutoff,” *Phys. Rev. D* **71** (2005) 036001, [arXiv:hep-ph/0407019](#).
- [4] L. Fromme, S. J. Huber, and M. Seniuch, “Baryogenesis in the two-Higgs doublet model,” *JHEP* **11** (2006) 038, [arXiv:hep-ph/0605242](#).
- [5] C. Grojean and G. Servant, “Gravitational Waves from Phase Transitions at the Electroweak Scale and Beyond,” *Phys. Rev. D* **75** (2007) 043507, [arXiv:hep-ph/0607107](#).
- [6] S. Profumo, M. J. Ramsey-Musolf, and G. Shaughnessy, “Singlet Higgs phenomenology and the electroweak phase transition,” *JHEP* **08** (2007) 010, [arXiv:0705.2425 \[hep-ph\]](#).
- [7] V. Barger, P. Langacker, M. McCaskey, M. J. Ramsey-Musolf, and G. Shaughnessy, “LHC Phenomenology of an Extended Standard Model with a Real Scalar Singlet,” *Phys. Rev. D* **77** (2008) 035005, [arXiv:0706.4311 \[hep-ph\]](#).
- [8] C. Delaunay, C. Grojean, and J. D. Wells, “Dynamics of Non-renormalizable Electroweak Symmetry Breaking,” *JHEP* **04** (2008) 029, [arXiv:0711.2511 \[hep-ph\]](#).
- [9] P. Fileviez Perez, H. H. Patel, M. J. Ramsey-Musolf, and K. Wang, “Triplet Scalars and Dark Matter at the LHC,” *Phys. Rev. D* **79** (2009) 055024, [arXiv:0811.3957 \[hep-ph\]](#).
- [10] G. Gil, P. Chankowski, and M. Krawczyk, “Inert Dark Matter and Strong Electroweak Phase Transition,” *Phys. Lett. B* **717** (2012) 396–402, [arXiv:1207.0084 \[hep-ph\]](#).
- [11] G. C. Dorsch, S. J. Huber, and J. M. No, “A strong electroweak phase transition in the 2HDM after LHC8,” *JHEP* **10** (2013) 029, [arXiv:1305.6610 \[hep-ph\]](#).
- [12] F. P. Huang, Y. Wan, D.-G. Wang, Y.-F. Cai, and X. Zhang, “Hearing the echoes of electroweak baryogenesis with gravitational wave detectors,” *Phys. Rev. D* **94** no. 4, (2016) 041702, [arXiv:1601.01640 \[hep-ph\]](#).
- [13] R. Jinno and M. Takimoto, “Probing a classically conformal B-L model with gravitational waves,” *Phys. Rev. D* **95** no. 1, (2017) 015020, [arXiv:1604.05035 \[hep-ph\]](#).
- [14] W. Chao, H.-K. Guo, and J. Shu, “Gravitational Wave Signals of Electroweak Phase Transition Triggered by Dark Matter,” *JCAP* **09** (2017) 009, [arXiv:1702.02698 \[hep-ph\]](#).
- [15] A. Beniwal, M. Lewicki, J. D. Wells, M. White, and A. G. Williams, “Gravitational wave,

- collider and dark matter signals from a scalar singlet electroweak baryogenesis,” *JHEP* **08** (2017) 108, [arXiv:1702.06124 \[hep-ph\]](#).
- [16] L. Marzola, A. Racioppi, and V. Vaskonen, “Phase transition and gravitational wave phenomenology of scalar conformal extensions of the Standard Model,” *Eur. Phys. J. C* **77** no. 7, (2017) 484, [arXiv:1704.01034 \[hep-ph\]](#).
- [17] G. Kurup and M. Perelstein, “Dynamics of Electroweak Phase Transition In Singlet-Scalar Extension of the Standard Model,” *Phys. Rev. D* **96** no. 1, (2017) 015036, [arXiv:1704.03381 \[hep-ph\]](#).
- [18] Y. Chen, M. Huang, and Q.-S. Yan, “Gravitation waves from QCD and electroweak phase transitions,” *JHEP* **05** (2018) 178, [arXiv:1712.03470 \[hep-ph\]](#).
- [19] I. Baldes and C. Garcia-Cely, “Strong gravitational radiation from a simple dark matter model,” *JHEP* **05** (2019) 190, [arXiv:1809.01198 \[hep-ph\]](#).
- [20] T. Prokopec, J. Rezaeck, and B. Świeżewska, “Gravitational waves from conformal symmetry breaking,” *JCAP* **02** (2019) 009, [arXiv:1809.11129 \[hep-ph\]](#).
- [21] L. Bian and X. Liu, “Two-step strongly first-order electroweak phase transition modified FIMP dark matter, gravitational wave signals, and the neutrino mass,” *Phys. Rev. D* **99** no. 5, (2019) 055003, [arXiv:1811.03279 \[hep-ph\]](#).
- [22] C. Marzo, L. Marzola, and V. Vaskonen, “Phase transition and vacuum stability in the classically conformal B–L model,” *Eur. Phys. J. C* **79** no. 7, (2019) 601, [arXiv:1811.11169 \[hep-ph\]](#).
- [23] M. Chala, M. Ramos, and M. Spannowsky, “Gravitational wave and collider probes of a triplet Higgs sector with a low cutoff,” *Eur. Phys. J. C* **79** no. 2, (2019) 156, [arXiv:1812.01901 \[hep-ph\]](#).
- [24] R. Zhou, W. Cheng, X. Deng, L. Bian, and Y. Wu, “Electroweak phase transition and Higgs phenomenology in the Georgi-Machacek model,” *JHEP* **01** (2019) 216, [arXiv:1812.06217 \[hep-ph\]](#).
- [25] A. Alves, T. Ghosh, H.-K. Guo, K. Sinha, and D. Vagie, “Collider and Gravitational Wave Complementarity in Exploring the Singlet Extension of the Standard Model,” *JHEP* **04** (2019) 052, [arXiv:1812.09333 \[hep-ph\]](#).
- [26] A. Azatov, D. Barducci, and F. Sgarlata, “Gravitational traces of broken gauge symmetries,” *JCAP* **07** (2020) 027, [arXiv:1910.01124 \[hep-ph\]](#).
- [27] L. Delle Rose, G. Panico, M. Redi, and A. Tesi, “Gravitational Waves from Supercool Axions,” *JHEP* **04** (2020) 025, [arXiv:1912.06139 \[hep-ph\]](#).
- [28] B. Von Harling, A. Pomarol, O. Pujolàs, and F. Rompineve, “Peccei-Quinn Phase Transition at LIGO,” *JHEP* **04** (2020) 195, [arXiv:1912.07587 \[hep-ph\]](#).
- [29] J. Halverson, C. Long, A. Maiti, B. Nelson, and G. Salinas, “Gravitational waves from dark Yang-Mills sectors,” *JHEP* **05** (2021) 154, [arXiv:2012.04071 \[hep-ph\]](#).

- [30] T. Ghosh, H.-K. Guo, T. Han, and H. Liu, “Electroweak phase transition with an SU(2) dark sector,” *JHEP* **07** (2021) 045, [arXiv:2012.09758 \[hep-ph\]](#).
- [31] W.-C. Huang, M. Reichert, F. Sannino, and Z.-W. Wang, “Testing the dark SU(N) Yang-Mills theory confined landscape: From the lattice to gravitational waves,” *Phys. Rev. D* **104** no. 3, (2021) 035005, [arXiv:2012.11614 \[hep-ph\]](#).
- [32] P. Di Bari, D. Marfatia, and Y.-L. Zhou, “Gravitational waves from first-order phase transitions in Majoron models of neutrino mass,” *JHEP* **10** (2021) 193, [arXiv:2106.00025 \[hep-ph\]](#).
- [33] M. Kierkla, A. Karam, and B. Swiezevska, “Conformal model for gravitational waves and dark matter: a status update,” *JHEP* **03** (2023) 007, [arXiv:2210.07075 \[astro-ph.CO\]](#).
- [34] E. Morgante, N. Ramberg, and P. Schwaller, “Gravitational waves from dark SU(3) Yang-Mills theory,” *Phys. Rev. D* **107** no. 3, (2023) 036010, [arXiv:2210.11821 \[hep-ph\]](#).
- [35] K. Fujikura, Y. Nakai, R. Sato, and Y. Wang, “Cosmological phase transitions in composite Higgs models,” *JHEP* **09** (2023) 053, [arXiv:2306.01305 \[hep-ph\]](#).
- [36] M. T. Frandsen, M. Heikinheimo, M. Rosenlyst, M. E. Thing, and K. Tuominen, “Gravitational waves from SU(N)/SP(N) composite Higgs models,” *JHEP* **09** (2023) 022, [arXiv:2302.09104 \[hep-ph\]](#).
- [37] R. Pasechnik, M. Reichert, F. Sannino, and Z.-W. Wang, “Gravitational waves from composite dark sectors,” *JHEP* **02** (2024) 159, [arXiv:2309.16755 \[hep-ph\]](#).
- [38] W.-Z. Feng, J. Li, and P. Nath, “Cosmologically consistent analysis of gravitational waves from hidden sectors,” *Phys. Rev. D* **110** no. 1, (2024) 015020, [arXiv:2403.09558 \[hep-ph\]](#).
- [39] F. Gao, S. Sun, and G. White, “A first-order deconfinement phase transition in the early universe and gravitational waves,” [arXiv:2405.00490 \[hep-ph\]](#).
- [40] F. Gao, J. Harz, C. Hati, Y. Lu, I. M. Oldengott, and G. White, “Baryogenesis and first-order QCD transition with gravitational waves from a large lepton asymmetry,” [arXiv:2407.17549 \[hep-ph\]](#).
- [41] E. Witten, “Cosmic Separation of Phases,” *Phys. Rev. D* **30** (1984) 272–285.
- [42] C. J. Hogan, “Gravitational radiation from cosmological phase transitions,” *Mon. Not. Roy. Astron. Soc.* **218** no. 4, (1986) 629–636.
- [43] A. Kosowsky and M. S. Turner, “Gravitational radiation from colliding vacuum bubbles: envelope approximation to many bubble collisions,” *Phys. Rev. D* **47** (1993) 4372–4391, [arXiv:astro-ph/9211004](#).
- [44] A. Kosowsky, M. S. Turner, and R. Watkins, “Gravitational waves from first order cosmological phase transitions,” *Phys. Rev. Lett.* **69** (1992) 2026–2029.
- [45] M. Kamionkowski, A. Kosowsky, and M. S. Turner, “Gravitational radiation from first

- order phase transitions,” *Phys. Rev. D* **49** (1994) 2837–2851, [arXiv:astro-ph/9310044](#).
- [46] V. A. Kuzmin, V. A. Rubakov, and M. E. Shaposhnikov, “On the Anomalous Electroweak Baryon Number Nonconservation in the Early Universe,” *Phys. Lett. B* **155** (1985) 36.
- [47] D. E. Morrissey and M. J. Ramsey-Musolf, “Electroweak baryogenesis,” *New J. Phys.* **14** (2012) 125003, [arXiv:1206.2942 \[hep-ph\]](#).
- [48] B. Garbrecht, “Why is there more matter than antimatter? Computational methods for leptogenesis and electroweak baryogenesis,” *Prog. Part. Nucl. Phys.* **110** (2020) 103727, [arXiv:1812.02651 \[hep-ph\]](#).
- [49] J. M. Cline and K. Kainulainen, “Electroweak baryogenesis at high bubble wall velocities,” *Phys. Rev. D* **101** no. 6, (2020) 063525, [arXiv:2001.00568 \[hep-ph\]](#).
- [50] A. Azatov, M. Vanvlasselaer, and W. Yin, “Baryogenesis via relativistic bubble walls,” *JHEP* **10** (2021) 043, [arXiv:2106.14913 \[hep-ph\]](#).
- [51] I. Baldes, S. Blasi, A. Mariotti, A. Sevrin, and K. Turbang, “Baryogenesis via relativistic bubble expansion,” *Phys. Rev. D* **104** no. 11, (2021) 115029, [arXiv:2106.15602 \[hep-ph\]](#).
- [52] P. Huang and K.-P. Xie, “Leptogenesis triggered by a first-order phase transition,” *JHEP* **09** (2022) 052, [arXiv:2206.04691 \[hep-ph\]](#).
- [53] E. J. Chun, T. P. Dutka, T. H. Jung, X. Nagels, and M. Vanvlasselaer, “Bubble-assisted leptogenesis,” *JHEP* **09** (2023) 164, [arXiv:2305.10759 \[hep-ph\]](#).
- [54] M. Cataldi and B. Shakya, “Leptogenesis via Bubble Collisions,” [arXiv:2407.16747 \[hep-ph\]](#).
- [55] A. Falkowski and J. M. No, “Non-thermal Dark Matter Production from the Electroweak Phase Transition: Multi-TeV WIMPs and ‘Baby-Zillas’,” *JHEP* **02** (2013) 034, [arXiv:1211.5615 \[hep-ph\]](#).
- [56] M. J. Baker, J. Kopp, and A. J. Long, “Filtered Dark Matter at a First Order Phase Transition,” *Phys. Rev. Lett.* **125** no. 15, (2020) 151102, [arXiv:1912.02830 \[hep-ph\]](#).
- [57] D. Chway, T. H. Jung, and C. S. Shin, “Dark matter filtering-out effect during a first-order phase transition,” *Phys. Rev. D* **101** no. 9, (2020) 095019, [arXiv:1912.04238 \[hep-ph\]](#).
- [58] W. Chao, X.-F. Li, and L. Wang, “Filtered pseudo-scalar dark matter and gravitational waves from first order phase transition,” *JCAP* **06** (2021) 038, [arXiv:2012.15113 \[hep-ph\]](#).
- [59] A. Azatov, M. Vanvlasselaer, and W. Yin, “Dark Matter production from relativistic bubble walls,” *JHEP* **03** (2021) 288, [arXiv:2101.05721 \[hep-ph\]](#).
- [60] A. Azatov, G. Barni, S. Chakraborty, M. Vanvlasselaer, and W. Yin, “Ultra-relativistic bubbles from the simplest Higgs portal and their cosmological consequences,” *JHEP* **10** (2022) 017, [arXiv:2207.02230 \[hep-ph\]](#).

- [61] I. Baldes, Y. Gouttenoire, and F. Sala, “Hot and heavy dark matter from a weak scale phase transition,” *SciPost Phys.* **14** no. 3, (2023) 033, [arXiv:2207.05096 \[hep-ph\]](#).
- [62] G. F. Giudice, H. M. Lee, A. Pomarol, and B. Shakya, “Nonthermal Heavy Dark Matter from a First-Order Phase Transition,” [arXiv:2403.03252 \[hep-ph\]](#).
- [63] A. Azatov, X. Nagels, M. Vanvlasselaer, and W. Yin, “Populating secluded dark sector with ultra-relativistic bubbles,” [arXiv:2406.12554 \[hep-ph\]](#).
- [64] W.-Y. Ai, M. Fairbairn, K. Mimasu, and T. You, “Non-thermal production of heavy vector dark matter from relativistic bubble walls,” [arXiv:2406.20051 \[hep-ph\]](#).
- [65] M. Barroso Mancha, T. Prokopec, and B. Swiezewska, “Field-theoretic derivation of bubble-wall force,” *JHEP* **01** (2021) 070, [arXiv:2005.10875 \[hep-th\]](#).
- [66] A. Friedlander, I. Banta, J. M. Cline, and D. Tucker-Smith, “Wall speed and shape in singlet-assisted strong electroweak phase transitions,” *Phys. Rev. D* **103** no. 5, (2021) 055020, [arXiv:2009.14295 \[hep-ph\]](#).
- [67] S. Balaji, M. Spannowsky, and C. Tamarit, “Cosmological bubble friction in local equilibrium,” *JCAP* **03** (2021) 051, [arXiv:2010.08013 \[hep-ph\]](#).
- [68] J. M. Cline, A. Friedlander, D.-M. He, K. Kainulainen, B. Laurent, and D. Tucker-Smith, “Baryogenesis and gravity waves from a UV-completed electroweak phase transition,” *Phys. Rev. D* **103** no. 12, (2021) 123529, [arXiv:2102.12490 \[hep-ph\]](#).
- [69] Y. Bea, J. Casalderrey-Solana, T. Giannakopoulos, D. Mateos, M. Sanchez-Garitaonandia, and M. Zilhão, “Bubble wall velocity from holography,” *Phys. Rev. D* **104** no. 12, (2021) L121903, [arXiv:2104.05708 \[hep-th\]](#).
- [70] F. Bigazzi, A. Caddeo, T. Canneti, and A. L. Cotrone, “Bubble wall velocity at strong coupling,” *JHEP* **08** (2021) 090, [arXiv:2104.12817 \[hep-ph\]](#).
- [71] W.-Y. Ai, B. Garbrecht, and C. Tamarit, “Bubble wall velocities in local equilibrium,” *JCAP* **03** no. 03, (2022) 015, [arXiv:2109.13710 \[hep-ph\]](#).
- [72] M. Lewicki, M. Merchand, and M. Zych, “Electroweak bubble wall expansion: gravitational waves and baryogenesis in Standard Model-like thermal plasma,” *JHEP* **02** (2022) 017, [arXiv:2111.02393 \[astro-ph.CO\]](#).
- [73] G. C. Dorsch, S. J. Huber, and T. Konstandin, “A sonic boom in bubble wall friction,” *JCAP* **04** no. 04, (2022) 010, [arXiv:2112.12548 \[hep-ph\]](#).
- [74] S. De Curtis, L. D. Rose, A. Guiggiani, A. G. Muyor, and G. Panico, “Bubble wall dynamics at the electroweak phase transition,” *JHEP* **03** (2022) 163, [arXiv:2201.08220 \[hep-ph\]](#).
- [75] B. Laurent and J. M. Cline, “First principles determination of bubble wall velocity,” *Phys. Rev. D* **106** no. 2, (2022) 023501, [arXiv:2204.13120 \[hep-ph\]](#).
- [76] S.-J. Wang and Z.-Y. Yuwen, “Hydrodynamic backreaction force of cosmological bubble expansion,” *Phys. Rev. D* **107** no. 2, (2023) 023501, [arXiv:2205.02492 \[hep-ph\]](#).

- [77] M. Lewicki, V. Vaskonen, and H. Veermäe, “Bubble dynamics in fluids with N-body simulations,” *Phys. Rev. D* **106** no. 10, (2022) 103501, [arXiv:2205.05667 \[astro-ph.CO\]](#).
- [78] R. A. Janik, M. Jarvinen, H. Soltanpanahi, and J. Sonnenschein, “Perfect Fluid Hydrodynamic Picture of Domain Wall Velocities at Strong Coupling,” *Phys. Rev. Lett.* **129** no. 8, (2022) 081601, [arXiv:2205.06274 \[hep-th\]](#).
- [79] L. Li, S.-J. Wang, and Z.-Y. Yuwen, “Bubble expansion at strong coupling,” *Phys. Rev. D* **108** no. 9, (2023) 096033, [arXiv:2302.10042 \[hep-th\]](#).
- [80] W.-Y. Ai, B. Laurent, and J. van de Vis, “Model-independent bubble wall velocities in local thermal equilibrium,” *JCAP* **07** (2023) 002, [arXiv:2303.10171 \[astro-ph.CO\]](#).
- [81] T. Krajewski, M. Lewicki, and M. Zych, “Hydrodynamical constraints on the bubble wall velocity,” *Phys. Rev. D* **108** no. 10, (2023) 103523, [arXiv:2303.18216 \[astro-ph.CO\]](#).
- [82] L. Giombi and M. Hindmarsh, “General relativistic bubble growth in cosmological phase transitions,” *JCAP* **03** (2024) 059, [arXiv:2307.12080 \[astro-ph.CO\]](#).
- [83] J.-C. Wang, Z.-Y. Yuwen, Y.-S. Hao, and S.-J. Wang, “General backreaction force of cosmological bubble expansion,” *Phys. Rev. D* **110** no. 1, (2024) 016031, [arXiv:2310.07691 \[hep-ph\]](#).
- [84] G. C. Dorsch and D. A. Pinto, “Bubble wall velocities with an extended fluid Ansatz,” *JCAP* **04** (2024) 027, [arXiv:2312.02354 \[hep-ph\]](#).
- [85] M. Sanchez-Garitaonandia and J. van de Vis, “Prediction of the bubble wall velocity for a large jump in degrees of freedom,” *Phys. Rev. D* **110** no. 2, (2024) 023509, [arXiv:2312.09964 \[hep-ph\]](#).
- [86] S. De Curtis, L. Delle Rose, A. Guiggiani, A. Gil Muyor, and G. Panico, “Non-linearities in cosmological bubble wall dynamics,” *JHEP* **05** (2024) 009, [arXiv:2401.13522 \[hep-ph\]](#).
- [87] Z. Kang and J. Zhu, “Confinement Bubble Wall Velocity via Quasiparticle Determination,” [arXiv:2401.03849 \[hep-ph\]](#).
- [88] D.-W. Wang, Q.-S. Yan, and M. Huang, “Bubble wall velocity and gravitational wave in the minimal left-right symmetric model,” *Phys. Rev. D* **110** no. 7, (2024) 076011, [arXiv:2405.01949 \[gr-qc\]](#).
- [89] N. Evans and W. Fan, “Designer bubble walls in a holographic Weyl semi-metal with magnetic field,” [arXiv:2408.10835 \[hep-th\]](#).
- [90] Z.-Y. Yuwen, J.-C. Wang, and S.-J. Wang, “Bubble wall velocity from number density current in (non)equilibrium,” [arXiv:2409.20045 \[hep-ph\]](#).
- [91] A. Ekstedt, O. Gould, J. Hirvonen, B. Laurent, L. Niemi, P. Schicho, and J. van de Vis, “How fast does the WallGo? A package for computing wall velocities in first-order phase transitions,” [arXiv:2411.04970 \[hep-ph\]](#).

- [92] G. D. Moore and T. Prokopec, “How fast can the wall move? A Study of the electroweak phase transition dynamics,” *Phys. Rev. D* **52** (1995) 7182–7204, [arXiv:hep-ph/9506475](#).
- [93] G. D. Moore and T. Prokopec, “Bubble wall velocity in a first order electroweak phase transition,” *Phys. Rev. Lett.* **75** (1995) 777–780, [arXiv:hep-ph/9503296](#).
- [94] B.-H. Liu, L. D. McLerran, and N. Turok, “Bubble nucleation and growth at a baryon number producing electroweak phase transition,” *Phys. Rev. D* **46** (1992) 2668–2688.
- [95] G. C. Dorsch, S. J. Huber, and T. Konstandin, “Bubble wall velocities in the Standard Model and beyond,” *JCAP* **12** (2018) 034, [arXiv:1809.04907 \[hep-ph\]](#).
- [96] X. Wang, F. P. Huang, and X. Zhang, “Bubble wall velocity beyond leading-log approximation in electroweak phase transition,” [arXiv:2011.12903 \[hep-ph\]](#).
- [97] B. Laurent and J. M. Cline, “Fluid equations for fast-moving electroweak bubble walls,” *Phys. Rev. D* **102** no. 6, (2020) 063516, [arXiv:2007.10935 \[hep-ph\]](#).
- [98] S. Jiang, F. P. Huang, and X. Wang, “Bubble wall velocity during electroweak phase transition in the inert doublet model,” *Phys. Rev. D* **107** no. 9, (2023) 095005, [arXiv:2211.13142 \[hep-ph\]](#).
- [99] J. Ignatius, K. Kajantie, H. Kurki-Suonio, and M. Laine, “The growth of bubbles in cosmological phase transitions,” *Phys. Rev. D* **49** (1994) 3854–3868, [arXiv:astro-ph/9309059](#).
- [100] A. F. Heckler, “The Effects of electroweak phase transition dynamics on baryogenesis and primordial nucleosynthesis,” *Phys. Rev. D* **51** (1995) 405–428, [arXiv:astro-ph/9407064](#).
- [101] H. Kurki-Suonio and M. Laine, “Real time history of the cosmological electroweak phase transition,” *Phys. Rev. Lett.* **77** (1996) 3951–3954, [arXiv:hep-ph/9607382](#).
- [102] J. R. Espinosa, T. Konstandin, J. M. No, and G. Servant, “Energy Budget of Cosmological First-order Phase Transitions,” *JCAP* **06** (2010) 028, [arXiv:1004.4187 \[hep-ph\]](#).
- [103] S. J. Huber and M. Sopena, “The bubble wall velocity in the minimal supersymmetric light stop scenario,” *Phys. Rev. D* **85** (2012) 103507, [arXiv:1112.1888 \[hep-ph\]](#).
- [104] S. J. Huber and M. Sopena, “An efficient approach to electroweak bubble velocities,” [arXiv:1302.1044 \[hep-ph\]](#).
- [105] T. Konstandin and J. M. No, “Hydrodynamic obstruction to bubble expansion,” *JCAP* **02** (2011) 008, [arXiv:1011.3735 \[hep-ph\]](#).
- [106] D. Bodeker and G. D. Moore, “Can electroweak bubble walls run away?,” *JCAP* **05** (2009) 009, [arXiv:0903.4099 \[hep-ph\]](#).
- [107] D. Bodeker and G. D. Moore, “Electroweak Bubble Wall Speed Limit,” *JCAP* **05** (2017) 025, [arXiv:1703.08215 \[hep-ph\]](#).
- [108] S. Höche, J. Kozaczuk, A. J. Long, J. Turner, and Y. Wang, “Towards an all-orders calculation of the electroweak bubble wall velocity,” *JCAP* **03** (2021) 009,

- [arXiv:2007.10343 \[hep-ph\]](#).
- [109] A. Azatov and M. Vanvlasselaer, “Bubble wall velocity: heavy physics effects,” *JCAP* **01** (2021) 058, [arXiv:2010.02590 \[hep-ph\]](#).
 - [110] Y. Gouttenoire, R. Jinno, and F. Sala, “Friction pressure on relativistic bubble walls,” *JHEP* **05** (2022) 004, [arXiv:2112.07686 \[hep-ph\]](#).
 - [111] I. Garcia Garcia, G. Koszegi, and R. Petrossian-Byrne, “Reflections on bubble walls,” *JHEP* **09** (2023) 013, [arXiv:2212.10572 \[hep-ph\]](#).
 - [112] W.-Y. Ai, “Logarithmically divergent friction on ultrarelativistic bubble walls,” *JCAP* **10** (2023) 052, [arXiv:2308.10679 \[hep-ph\]](#).
 - [113] S. De Curtis, L. Delle Rose, A. Guiggiani, A. Gil Muyor, and G. Panico, “Collision integrals for cosmological phase transitions,” *JHEP* **05** (2023) 194, [arXiv:2303.05846 \[hep-ph\]](#).
 - [114] W.-Y. Ai, X. Nagels, and M. Vanvlasselaer, “Criterion for ultra-fast bubble walls: the impact of hydrodynamic obstruction,” *JCAP* **03** (2024) 037, [arXiv:2401.05911 \[hep-ph\]](#).
 - [115] L. Leitaó and A. Megevand, “Hydrodynamics of phase transition fronts and the speed of sound in the plasma,” *Nucl. Phys. B* **891** (2015) 159–199, [arXiv:1410.3875 \[hep-ph\]](#).
 - [116] M. Laine, “Bubble growth as a detonation,” *Phys. Rev. D* **49** (1994) 3847–3853, [arXiv:hep-ph/9309242](#).
 - [117] J. Kozaczuk, “Bubble Expansion and the Viability of Singlet-Driven Electroweak Baryogenesis,” *JHEP* **10** (2015) 135, [arXiv:1506.04741 \[hep-ph\]](#).
 - [118] J. R. Espinosa and M. Quiros, “The Electroweak phase transition with a singlet,” *Phys. Lett. B* **305** (1993) 98–105, [arXiv:hep-ph/9301285](#).
 - [119] J. R. Espinosa, T. Konstandin, and F. Riva, “Strong Electroweak Phase Transitions in the Standard Model with a Singlet,” *Nucl. Phys. B* **854** (2012) 592–630, [arXiv:1107.5441 \[hep-ph\]](#).
 - [120] L. Niemi, P. Schicho, and T. V. I. Tenkanen, “Singlet-assisted electroweak phase transition at two loops,” *Phys. Rev. D* **103** no. 11, (2021) 115035, [arXiv:2103.07467 \[hep-ph\]](#). [Erratum: *Phys.Rev.D* 109, 039902 (2024)].
 - [121] O. Gould and T. V. I. Tenkanen, “On the perturbative expansion at high temperature and implications for cosmological phase transitions,” *JHEP* **06** (2021) 069, [arXiv:2104.04399 \[hep-ph\]](#).
 - [122] M. Lewicki, M. Merchand, L. Sagunski, P. Schicho, and D. Schmitt, “Impact of theoretical uncertainties on model parameter reconstruction from GW signals sourced by cosmological phase transitions,” *Phys. Rev. D* **110** no. 2, (2024) 023538, [arXiv:2403.03769 \[hep-ph\]](#).
 - [123] A. Dashko and A. Ekstedt, “Bubble-wall speed with loop corrections,”

[arXiv:2411.05075 \[hep-ph\]](#).

- [124] W.-Y. Ai, M. Carosi, B. Garbrech, C. Tamarit, and M. Vanvlasselaer, “Bubble wall dynamics from non-equilibrium quantum field theory.” *forthcoming*.
- [125] F. Giese, T. Konstandin, and J. van de Vis, “Model-independent energy budget of cosmological first-order phase transitions—A sound argument to go beyond the bag model,” *JCAP* **07** no. 07, (2020) 057, [arXiv:2004.06995 \[astro-ph.CO\]](#).
- [126] F. Giese, T. Konstandin, K. Schmitz, and J. van de Vis, “Model-independent energy budget for LISA,” *JCAP* **01** (2021) 072, [arXiv:2010.09744 \[astro-ph.CO\]](#).